# Sulfur Isotope Measurement of Sulfate and Sulfide by High-Resolution MC-ICP-MS

Paul R. Craddock[a*], Olivier J. Rouxel[b], Lary A. Ball[b,1] and Wolfgang Bach[b,2]

[a] *Massachusetts Institute of Technology/Woods Hole Oceanographic Institution Joint Program in Chemical Oceanography, Woods Hole Oceanographic Institution, 360 Woods Hole Road, McLean 201, MS#8, Woods Hole, MA 02543, USA*

*Email: pcraddock@whoi.edu, Tel: 1-508-289-3712, Fax: 1-508-457-2159*

** Corresponding author*

[b] *Department of Marine Chemistry and Geochemistry, Woods Hole Oceanographic Institution, 360 Woods Hole Road, Woods Hole, MA 02543, USA.*

*Email: orouxel@whoi.edu*

[1] *Present address: Thermo Fisher Scientific, Inc., 53 Old Main Rd, North Falmouth, MA 02556, USA.*

*Email: lary.ball@thermofisher.com.*

[2] *Present address: University of Bremen, Geosciences Department, Klagenfurter Strasse, 28359, Bremen, Germany.*

*Email: wbach@uni-bremen.de*

# Abstract

We have developed a technique for the accurate and precise determination of $^{34}S/^{32}S$ isotope ratios ($\delta^{34}S$) in sulfur-bearing minerals using solution and laser ablation multiple-collector inductively coupled plasma mass spectrometry (MC-ICP-MS). We have examined and determined rigorous corrections for analytical difficulties such as instrumental mass bias, unresolved isobaric interferences, blanks, and laser ablation- and matrix-induced isotopic fractionation. Use of high resolution sector-field mass spectrometry removes major isobaric interferences from $O_2^+$. Standard–sample bracketing is used to correct for the instrumental mass bias of unknown samples. Blanks on sulfur masses arising from memory effects and residual oxygen-tailing are typically minor (< 0.2 ‰, within analytical error), and are mathematically removed by on-peak zero subtraction and by bracketing of samples with standards determined at the same signal intensity (within 20 %). Matrix effects are significant (up to 0.7 ‰) for matrix compositions relevant to many natural sulfur-bearing minerals. For solution analysis, sulfur isotope compositions are best determined using purified (matrix-clean) sulfur standards and sample solutions using the chemical purification protocol we present. For in situ analysis, where the complex matrix cannot be removed prior to analysis, appropriately matrix-matching standards and samples removes matrix artifacts and yields sulfur isotope ratios consistent with conventional techniques using matrix-clean analytes. Our method enables solid samples to be calibrated against aqueous standards; a consideration that is important when certified, isotopically-homogeneous and appropriately matrix-matched solid standards do not exist. Further, bulk and in situ analyses can be performed interchangeably in a single analytical session because the instrumental setup is identical for both. We validated the robustness of our analytical method through multiple isotope analyses of a range of reference materials and have compared these with isotope ratios determined using independent techniques. Long-term reproducibility of S isotope compositions is typically 0.20 ‰ and 0.45 ‰ (2σ) for solution and laser analysis, respectively. Our method affords the opportunity to make accurate and relatively precise S isotope measurement for a wide range of sulfur-bearing materials, and is particularly appropriate for geologic samples with complex matrix and for which high-resolution in situ analysis is critical.

*Keywords*

Sulfur, Isotope Composition, ICP, Mass Spectrometry, Laser Ablation

## 1. Introduction

Sulfur is widely distributed throughout the environment. Principally, sulfur occurs as sulfate in open, oxygenated seawater, while $H_2S$ and other reduced sulfide species reside in anoxic basins and sediment porewaters. In sediments, igneous and metamorphic rocks and metal-rich ore deposits, sulfur occurs in various oxidation states, such as sulfate, elemental sulfur and numerous metal sulfides. Variations in sulfur isotopic compositions of these reservoirs can be large (on the order of $\delta^{34}S \sim 20 - 50$ ‰ (Faure, 1986; Hoefs, 1997)) and so they serve as key tracers of sources and cycling of sulfur species in biological and geochemical processes (Thode et al., 1961; Goldhaber and Kaplan, 1974; Ohmoto and Rye, 1979; Canfield, 2001; Shanks, 2001).

Conventionally, measurements of sulfur isotope ratios are performed using gas-source mass spectrometry (GS-MS) in which sulfur is introduced as gaseous $SO_2$ or $SF_6$ (Thode et al., 1961; Fritz et al., 1974; Robinson and Kusakabe, 1975; Rees, 1978). The latter is preferred for high-precision S isotope analysis because $SF_6$ has no spectral interferences from oxygen species and no memory effects (Rees, 1978). However, sample preparation for GS-MS is complex and time-consuming (Thode et al., 1961). Online elemental-analyzer isotope-ratio mass spectrometry (EA-IRMS) has been more recently developed to automate the combustion formation and chromatographic purification procedures for a $SO_2$ gas source (Giesemann et al., 1994; Grassineau et al., 2001; Studley et al., 2002) and is now a widely-used technique for sulfur isotopic measurements. This approach has reduced minimum sample mass requirements (< 1 mg S) and expedited sample throughput. For GS-MS, $\delta^{34}S$ ratios are commonly determined on masses 66 ($^{34}S^{16}O_2^+$) and 64 ($^{32}S^{16}O_2^+$). Variations of $^{18}O/^{16}O$ contributing to the isotopic composition of the $SO_2$ analyte are often not reproducible and poorly constrained using automated preparation systems and have resulted in calculated $\delta^{34}S$ values in error by up to 1 – 3 ‰ (Fry et al., 2002). Thus, manual preparation of $SO_2$ is still required in many cases in order to obtain the necessary precision and accuracy for S isotope analysis. A procedure that minimizes sampling handling and accelerates analysis, but enables high-precision isotope measurements, is highly desirable.

Alternative methods, such as ion microprobe (Chaussidon et al., 1987; Eldridge et al., 1987; Paterson et al., 1997; Mojzsis et al., 2003) and laser probe coupled to GS-MS (Shanks et al., 1998; Hu et al., 2003) have been developed for in situ measurement of S isotopes at increased spatial resolution to obtain information about biogeochemical processes that cannot be gained through bulk analytical measurements. These techniques alleviate the need for extensive sample preparation and so reduce minimum sample size and expedite sample throughput. However, they are subject to shortcomings including significant instrumental mass bias resulting from matrix effects. Consequently, it is necessary to have isotopically homogeneous and well-characterized, matrix-matched mineral standards, which are not available for all materials (Paterson et al., 1997; Riciputi et al., 1998). Multiple-collector thermal ionization mass spectrometry (MC-TIMS) has also been examined to measure precise S isotope ratios (Mann and Kelly, 2005). The use of a sulfur double-spike as an internal standard for MC-TIMS alleviates the need for homogeneous, matrix-matched external standards (Mann and Kelly, 2005). This method allows precise determination of S isotope ratios at small sample sizes (< 100 μg S). However, the addition of the double-spike technique requires the sample be in solution form and so the benefits of in situ analysis without sample preparation are lost.

Inductively coupled plasma mass spectrometry (ICP-MS) is increasingly becoming used as a tool for the measurement of stable isotope systems (Halliday et al., 1998; Albarède and Beard, 2004; Anbar and Rouxel, 2007). ICP-MS instruments are compatible with numerous sample introduction schemes, including solution (*bulk*) analysis and laser-ablation (*in situ*) analysis, which are not available for other techniques. ICP-MS represents a promising technique for the analysis of sulfur isotopes at sample masses (~ 10 µg S) similar to other techniques (Menegário et al., 1998; Mason et al., 1999; Prohaska et al., 1999; Krupp et al., 2004; You and Li, 2005; Clough et al., 2006; Mason et al., 2006). Measurement of S isotopes by single-collector ICP-MS is obtained sequentially and vriability of plasma conditions (e.g., efficiency of ionization, ion beam extraction) can significantly degrade the measurement of isotope ratios. The overall precision achievable by this method is typically greater than 2 to 5 ‰ (Jarvis et al., 1992; Menegário et al., 1998; Evans et al., 2001) and is not sufficient to resolve all sulfur isotope variations occurring in nature. The introduction of multiple collector ICP-MS technology has enabled simultaneous measurement of multiple isotopes, providing precise and rapid isotope ratio determination. Precision better than 1 ‰ is now obtainable for $\delta^{34}$S isotope ratios (Clough et al., 2006; Mason et al., 2006). Implicit in the accurate and precise determination of isotope ratios by MC-ICP-MS is an appropriate correction for instrumental mass discrimination. To date, external normalization (Rehkämper and Halliday, 1998; Maréchal et al., 1999) using either $^{37}$Cl/$^{35}$Cl or $^{30}$Si/$^{29}$Si isotope spikes has been preferred for S isotopes studies (Clough et al., 2006; Mason et al., 2006). However, it has not been sufficiently demonstrated that external normalization is appropriate for mass bias correction for all sulfur-bearing samples with a range of matrix, particularly for laser ablation MC-ICP-MS where the matrix cannot be removed prior to analysis. Our limited understanding of the effects of matrix for S isotope determination greatly limits the current application of solution and laser ablation MC-ICP-MS .

Development of a new analytical technique for sulfur isotope measurement is motivated by the need for rapid, versatile, precise and accurate *in situ and bulk* characterization of *sulfate* (e.g., anhydrite, barite, gypsum) *and sulfide* minerals (e.g., pyrite, chalcopyrite), widespread in the environment. Here, we present a detailed description of sulfur isotope measurement of sulfate and sulfide by solution and laser-ablation MC-ICP-MS. We examine potential difficulties associated with this technique, including instrumental and laser-ablation induced mass fractionation, isobaric interferences, blank contributions and matrix effects, and detail approaches to correct for these artifacts, enabling higher-precision measurements. This new contribution affords the possibility to carry out accurate and precise S isotope measurements for a range of sulfur-bearing materials both by bulk analysis and in situ at sub-millimeter spatial scales and should be of interest to a variety of geological and geochemical studies.

## 2. Analytical Methods

### *2.1. Preparation of reagents, standards and blanks*

All bottles and vials used for sample preparation and storage were cleaned for a 24 h period in Fisher TraceMetal grade 20 % hydrochloric acid and rinsed three times with 18 MΩ cm Milli-Q water. All standard and sample solutions were prepared for analysis as matrix-matched, purified S solutions stabilized in 2 % (w/w) nitric acid ($HNO_3$). Either SeaStar Baseline$^{TM}$ (SeaStar Chemicals Inc., Sidney, BC Canada) or Fisher Optima$^{TM}$ (Fisher Scientific Co., Agawam, MA) ultra-pure $HNO_3$ was used. Milli-Q water used for dilutions was prepared using a Millipore Element de-ionizing unit operated at 18 MΩ cm.

Sulfur reference materials IAEA-S-1, S-2, S-4 and NBS-123 (Coplen and Krouse, 1998; Ding et al., 2001; Qi and Coplen, 2003) were used to calibrate laboratory (in-house) standards and to enable inter-laboratory comparison against the V-CDT scale.  Laboratory standard solutions ($S_{Alfa}$ and $S_{Spex}$) containing 20 ppm S were prepared from high-purity solutions and used throughout daily analytical sessions as the isotope reference. $S_{Alfa}$ was prepared by gravimetric dilution of an AlfaAesar Specpure$^{TM}$ 1000 µg ml$^{-1}$ S stock (Alfa Aesar, Johnson-Matthey Co., Ward Hill, MA) and $S_{Spex}$ by gravimetric dilution of a Spex CertiPrep$^{®}$ 10,000 µg ml$^{-1}$ S stock (SPEX CertiPrep Group, Metuchen, NJ). In addition, a range of geological reference samples with known isotope compositions were used as reference materials to enable comparison against isotope ratios determined using conventional analytical techniques. Two percent $HNO_3$ blank solutions were prepared from the same lot to quantify sulfur blanks throughout analytical sessions.

A mineral standard of anhydrite ($CaSO_4$; hereafter referred to as Sch-M-2) was prepared for laser ablation and bulk analysis in order to cross-calibrate solution and laser techniques. The Sch-M-2 solution was prepared by dissolving an appropriate mass of pure anhydrite in Milli-Q water and stabilizing the solution in ultra-pure 2 % $HNO_3$ acid to obtain a standard containing 20 ppm S. For laser ablation analysis, a 2 mm thick section was cut, polished and mounted onto a standard (45 x 25 mm) petrographic slide; no further preparation was necessary.

### *2.2. Chemical purification of reference standards and sulfide-sulfate samples*

Less than 50 mg of sample was accurately weighed into a 15ml PTFE digestion vessel. Samples were first reacted with 5 ml of $HNO_3$ (50 %) and taken to dryness on hot plate at less than 70 °C. Total digestion of the dry residue (containing abundant elemental sulfur) was obtained using 3 ml of concentrated $HNO_3$ and 2 mL of HCl (50 %). The solution was heated in the sealed PTFE container on a hot plate at a temperature of 70 °C and taken to dryness. The dry residue was fully dissolved with 4 mL of 2 % $HNO_3$. During dissolution of $Ag_2S$, insoluble white crystalline solids (presumably AgCl) precipitated and were separated from the solution by centrifugation.

A precise solution volume, corresponding to 500 μg of S, was then purified on a cation exchange chromatographic column AG50-X8 ($H^+$ form, Biorad, Hercules, CA, USA). The column was filled with 2.5 ml of resin (wet volume) and washed with 20 mL $H_2O$ and conditioned with 10 mL 1.4N $HNO_3$. The solution that passed through the column contains S and other oxyanions (e.g., silicic acid, phosphate, molybdate) whereas matrix elements (including sulfide- and sulfate-forming elements Fe, Ca, Cu, Zn) are strongly adsorbed on the resin. Complete recovery of S is assured after washing the column with 5 ml of 2 % $HNO_3$. The final solution was diluted with an appropriate amount of 2 % $HNO_3$ to obtain a final stock containing 50 ppm S.

Quantitative recovery of S is essential to avoid potential isotope fractionation of standards and samples during chemical processing. Loss of S can arise from volatilization of $H_2S$, or from the formation of insoluble sulfate or elemental sulfur. The former is unlikely as the use of strong oxidizing acids ($HNO_3$) during sample dissolution prevents the formation of volatile $H_2S$. Further, complete and repeated dissolution of sulfur-bearing particles is assured prior to column purification. Dissolution yields were evaluated for pyrite by measuring Fe/S ratios in solution prior to S purification. In all instances, molar S/Fe ratios in solutions were 1.95 ± 0.05, consistent with pyrite stoichiometry and indicate no loss of S. Complete recovery of S during column purification is ensured by passing S as sulfate through the AG50-X8 resin and washing with 5 ml of 2 % $HNO_3$. Yields of S are 98 ± 4 %, as calculated from purification of multiple, independent aliquots of the $S_{Alfa}$ in-house standard doped with matrix elements. The measured isotope compositions of the resulting purified standards are consistent within analytical uncertainties (see section 3.3). The procedural blank, resulting from chemical processing and purification is ~ 0.05 % (~ 0.25 µg per 500 µg S used for column chemistry).

### *2.3. Instrumentation and apparatus*

Isotopic measurements were performed using a NEPTUNE multiple collector inductively coupled plasma mass spectrometer (Thermo Fisher Scientific, Bremen, Germany) equipped with nine Faraday Cups. A NewWave UP213 Nd:YAG laser was used as the ablation source for analysis of solid samples. Instrument settings and typical operating parameters are summarized in Figure 1 and Table 1. Sulfur solutions are aspirated using Ar as the nebulizer gas. A laser ablation cyclonic spray dual chamber (a.k.a. Stable Sample Introduction System) and PFA-50 nebulizer (both from Elemental Scientific Inc., Omaha, NE) were used to introduce aerosols to the ICP torch. This spray chamber hosts an additional inlet to allow introduction of ablated material to the torch. The laser is connected directly to the spray chamber via 3 mm internal diameter Tygon tubing and uses He as the carrier gas from the laser to the ICP. The setup is such that laser ablation and solution aspiration can be operated simultaneously and enables laser particles to be efficiently mixed with an ultra-pure 2 % $HNO_3$ blank solution prior to injection into the ICP torch. Thus, laser particles are effectively analyzed as a ‘wet plasma’ ensuring that ablated aerosols are closely matrix-matched to solution standards. We opt not to use ‘dry’ plasma conditions (Mason et al., 2006) because this limits the application of the method to in situ analysis only. Sulfur is highly volatile and, therefore, passing solutions through a desolvating nebulizer to obtain dry plasma conditions is not viable for bulk analysis. Our setup allows for interchangeable bulk and in situ S isotope measurement.

Operating parameters for laser analysis are optimized in order to provide the most stable signal intensities during ablation. The laser is operated in apertured mode, with a spot size of 60 µm and a minimum total signal intensity of 10 volts ($^{32}$S signal). The power output of the laser is adjusted so as to ensure that the signal intensity of the ablated sample and bracketing solution standard are the same, typically with less than 20 % difference. A line scan (‘raster’) protocol is used in preference to a single crater mode in order to obtain a higher and more uniform rate of material removal with respect to time.  The raster mode utilizes a movable sample stage under a fixed laser beam to generate the desired raster pattern. The size of the trench formed during ablation is ~ 200 x 100 µm in cross-sectional area and ~ 250 µm deep. A scan speed of 5 µm s$^{-1}$ is used during ablation and yields an ablation removal rate for the sample of ~ 60 ng s$^{-1}$. Total acquisition time is ~ 4 minutes and results in ablation of ~ 15 µg of sample. The signal intensity is monitored to ensure that transport of sample into the ICP-MS does not significantly diminish as material is ablated during analysis.

### *2.4. Isotope measurement and data acquisition*

Isotope ratio measurements are performed in high mass resolution mode in order to separate sulfur from potential interfering species (Table 2). Isotopic measurements are performed on masses $^{32}S$, $^{33}S$ and $^{34}S$. Molecular interferences from $^{16,17,18}O_2$ are heavier than elemental species, so isotopes of sulfur are determined free from molecular interferences on the low mass shoulder of interfering species (Figure 2). Data are not reported for $^{36}S$ because of the low abundance of this isotope and interferences from Ar.

Each measurement consists of twenty cycles, each cycle having 8.5 second integration. Data acquisition for in situ analyses is initiated approximately 15 seconds after the laser is fired. This delay accounts for transport of ablated material into the mass spectrometer and the time taken to establish a stable signal on the Faraday cups. Similarly, data acquisition for solution analyses begins once a stable signal is established for the aspirated sample. Baseline intensities are measured for 5 seconds at the beginning of each analysis by deflecting the ion beams. Background interference is evaluated by measuring signal intensities on sulfur masses whilst aspirating blank (2 % nitric acid) solutions periodically throughout the analytical session (i.e., on-peak zero). On-peak background is measured on the low mass shoulder (identical to sample measurements) to avoid tailing from $O_2$ and negative background due to possible ion scattering on the sides of the Faraday Cup. Wash-out times of two minutes and four minutes are used following solution and laser ablation analysis, respectively (Table 2). Automatic rejection of outlying cycles (2σ outlier criterion) offered within the NEPTUNE software is not performed. All data acquired, including raw Faraday intensities, raw measured isotope ratios and corresponding standard deviations and standard errors for each measurement, are evaluated off-line.

Absolute S isotope ratios of unknown samples are determined using standard-sample bracketing (Belshaw et al., 1998; Albarède and Beard, 2004). The true S isotope ratio is calculated by correction for instrumental mass bias by linear interpolation between the biases calculated from two neighboring standard analyses. Isotope compositions are presented in the conventional delta (δ) notation by reference to in-house matrix-matched standards ($S_{Spex}$ and $S_{Alfa}$), i.e.;

$$\delta^{34}S = \left( \frac{(^{34}S/^{32}S)_{sample}}{(^{34}S/^{32}S)_{standard}} - 1 \right) \text{ x } 1000$$

Analogous relations are used for the determination of $\delta^{33}S$, substituting $^{33}S$ for $^{34}S$ in the equation above. The isotope compositions of in-house standards used to bracket unknown samples have been calibrated exactly against reference material IAEA-S-1. The S isotope compositions of samples are then normalized to the Vienna Cañon Diablo Troilite (V-CDT) scale assuming, by definition, $\delta^{34}S_{V\text{-}CDT}$ of IAEA-S-1 exactly equal to – 0.3 ‰ (Ding et al., 2001). Further calibration and verification of the 'accuracy' of the S isotope compositions of in-house standards was examined by determining the isotope compositions of other reference materials analyzed as unknowns. Within uncertainty, the isotope compositions of reference materials determined by this study are consistent with published consensus $\delta^{34}S$ values (Table 3). For individual analyses, internal precision is reported at the 1σ error level. For replicate analyses, external reproducibility is reported at the 2σ error level.

## 3. Experimental Results

### *3.1. Isobaric interference and background correction*

Isobaric interferences and blank contamination can contribute to measured signal intensities on sulfur isotope masses of interest and can bias measured isotope ratios. An assessment of these two artifacts is required in order to obtain the necessary precision and accuracy for S isotope measurements. Isobaric interferences include molecular ions (e.g., $^{16}O$-$^{16}O^+$, $^{32}S$-$^{1}H^+$ and $^{17}O$-$^{16}O$-$^{1}H^+$) and less abundant doubly-charged ions (e.g., $^{64}Zn^{2+}$) and exist on all isotopes of interest (Table 2). For accurate determination of S isotope ratios, it is essential that these interferences either be removed completely or be resolved with appropriate mass resolution. For the NEPTUNE, sulfur isotope measurements can be performed setting the entrance slit to medium or high resolution (high resolution recommended) and detector slit to low resolution. In this configuration, sulfur is resolved as a flat plateau (peak shoulder) on the low mass side of interfering oxygen species and the detector is positioned on this interference-free shoulder for data collection (Figure 2). The mass resolution for this setup is defined by the resolving power of the mass spectrometer, $m/\Delta m^*$ (Weyer and Schwieters, 2003). It is important to note that the resolving power ($m/\Delta m^*$) is distinct to standard mass resolution given by the 10 % valley definition, and is a factor of 3 – 4 higher than standard mass resolution (Weyer and Schwieters, 2003). A resolving power $m/\Delta m^* \sim 5000 – 6000$ is sufficient to separate major oxygen interferences, including contributions from oxygen-tailing and ion-scattering, from sulfur isotopes of interest.

The resolving power of the NEPTUNE is not sufficient to fully separate sulfur from hydride interferences ($m/\Delta m^* > 12,000$), and so hydride formation should be quantified. We calculate on average ~ 0.05 – 0.10 % production efficiency for sulfur hydride. For the low abundance isotope

$^{33}$S, contribution from $^{32}$S-$^{1}$H is more than 10 % of the total signal on mass 33, resulting in significant bias of the measured isotope ratio and poor reproducibility of $\delta^{33}$S ratios of about 2 – 3 ‰ (see section 3.2.). Hydride contribution from $^{33}$S-$^{1}$H$^{+}$ on mass 34 is negligible (< 0.02 %) and does not limit the overall precision for $^{34}$S/$^{32}$S ratios obtainable by this technique, in particular because the effect of hydride formation is corrected by the standard-sample bracketing technique. The rate of hydride formation is calculated for each measurement using ($^{33}$S + $^{32}$SH)/$^{32}$S vs. $^{34}$S/$^{32}$S relationship to ensure that hydride formation is uniform between sample and standard analysis.

Blank contributions can include sulfur due to laboratory contamination and from instrument memory. Previous high-precision S isotope ratio measurements by laser ablation lacked quantitative assessment of blanks (Mason et al., 2006). The procedural blank for our purification method was assessed during preparation and chemical purification of sulfur standards and samples. The blank is calculated to be ~ 0.05 % of total sulfur processed. Typically, sulfur intensities of the procedural blank are minor as compared to sulfur intensities of standards and samples (~ 30 mV for blank *versus* 15 – 20 V for standard, on mass 32). Further, sulfur contamination can result from transient memory effects during sulfur isotope measurement. These effects are manifest as small, but variable, spikes in the sulfur intensity during the aspiration of a blank solution after analysis of a sulfur-bearing analyte. Memory effects are not significant for solution-based analysis and are removed by applying a two minute wash-out period after solution analysis. However, they can be more important for laser ablation analysis because residual particles can be carried from the laser cell to the mass spectrometer for an extended period after ablation and isotope analysis have finished. Typically, a four minute wash-out period after in situ analysis is sufficient and recommended to enable spikes arising from residual particles to be removed.

Total background corrections are necessary if trace, but measurable, sulfur contamination or unresolved interferences contribute to signal intensities and bias isotope compositions. Repeated analyses of in-house sulfur standards at a range of sulfur concentration and signal intensity indicate significant deviation of measured S isotope ratios from true ratios at low sulfur concentration (Figure 3). Correction for total background is performed by periodic aspiration and isotopic measurement of blank solutions throughout each analytical session. Absolute signal intensity of the background is ~ 30 – 50 mV (on $^{32}S$). Average background intensities are determined for each isotope (on-peak zero) and are directly subtracted from the signal intensity for each sulfur isotope mass as part of off-line evaluation. For routine sample analysis, the necessary correction for background contributions is typically small (≤ 0.4 ‰), but can be variable. However, these deviations are statistically significant and can produce perturbations of S isotope ratios greater than 1.0 ‰ at less than one volt signal intensity (on $^{32}S$). Approaches to minimize the magnitude of the background correction required to within limits of analytical precision are advantageous because the concentration and isotopic composition of the blank are inherently variable and difficult to characterize. Accordingly, the following procedures are recommended; (1) measure isotope ratios of standard and sample analytes at minimum signal intensities ~ 10 volts (signal-to-background ratios > 300) and, (2) determine isotope compositions of unknown samples with a standard analyzed at the same intensity (within ~ 20 %). By closely matching signal intensities, the mass bias calculated for the standard accounting for effects of both instrumental fractionation and background can be directly applied to unknown samples.

### 3.2. Internal precision and instrument mass bias

In this study, we choose to apply the standard-sample bracketing technique to correct for instrumental mass discrimination. A matrix-matched sulfur solution is used as the bracketing standard for both bulk and in situ sample analysis. The magnitude and stability of instrumental mass bias is calculated from the evolution of the isotopic standard throughout the analytical session. For sulfur, we calculate typical mass bias between 4.0 and 5.1 % per atomic mass unit. Mass bias is variable between analytical sessions, but is generally stable to around 0.1 % over the duration of a single session and to 0.01 – 0.02 % between consecutive bracketing standards. The stability of this mass bias determines the ultimate precision obtainable by the standard-sample bracketing technique. Varying instrumental mass bias (i.e., drift) will increase the errors associated with applying mass bias corrections to unknown samples and will compromise analytical precision. We have assessed instrumental drift and observe no statistically significant deviation of isotope ratios (> 0.02 %) during routine analysis of individual samples, for analysis times up to approximately four minutes. Long-term drift, occurring over the duration of multiple sample analyses, is easily corrected by stringent standard-sample bracketing of unknown samples with standards analyzed immediately before and after. Data that show clear and large mass bias drift (greater than ~ 0.5 ‰) during individual samples should be discarded.

The overall precision of bulk S isotope analysis using standard-sample bracketing has been assessed from the long-term reproducibility of $S_{Spex}$ and $S_{Alfa}$ standard solutions measured over multiple, independent analytical sessions (Figure 4). For routine bulk analysis, we estimate an external precision of ± 0.21 ‰ (2σ) and ± 0.18 ‰ (2σ) for $\delta^{34}S_{Alfa}$ and $\delta^{34}S_{Spex}$, respectively (20 – 30 replicates). In contrast, the precision for $\delta^{33}S$ values deteriorate by an order of magnitude relative to $\delta^{34}S$ due to the large contribution and high variability of unresolved $^{32}S$-$^{1}H$ interference on $^{33}S$ (Figure 4). The external precision of in situ S isotope analysis is more difficult to assess because real isotopic heterogeneity may contribute to variability of isotope compositions determined by repeat analyses of mineral samples. An estimate of external precision of in situ techniques was determined by replicate analysis of the isotopically homogenous anhydrite standard Sch-M-2 and calculated to be ± 0.45 ‰ (2σ; 12 replicates).

### *3.3. Matrix effects*

Instrumental mass bias within ICP-MS results from so-called ‘space-charge’ and ‘ion-diffusion’ effects on the transmission of ionized particles (Tanner, 1992; Vanhaecke et al., 1993; Maréchal et al., 1999) and has been shown to be sensitive to matrix composition (Galy et al., 2003; Pietruszka et al., 2006). In order to evaluate the possibility of matrix effects from elements that are commonly found in sulfide and sulfate minerals, we performed doping experiments using $S_{spex}$ standard solution mixed with various high-purity element solutions. For each experiment, we used synthetic solutions with a matrix corresponding to stoichiometry of various sulfide and sulfate minerals (e.g. anhydrite, pyrite, chalcopyrite, sphalerite, etc.). The S isotope ratios of doped $S_{spex}$ solutions were determined and compared against the S isotope ratio of purified $S_{spex}$ solutions (Figure 5). The results show, in most cases, that matrix effects from Ca, Fe, Ni, Mo, Sn are significant (up to 0.7 ‰) and yield poorly reproducible isotope determination. The data also indicate that the presence of matrix elements tend to increase the instrumental mass bias for S.

In order to evaluate the efficiency of the chemical purification procedure to remove matrix elements, we separated and purified an aliquot of the doped solutions. The aliquots were processed through cation-exchange (AG50-X8) resin as described previously and re-analyzed as unknown samples. The results demonstrate that chemical purification effectively removes the matrix and enables consistent and reproducible isotope measurements free of matrix effects (Figure 5). Further, the data indicate that the chemical purification procedures do not introduce any artificial isotope fractionation (e.g., from loss of S) that would compromise the accuracy of this method. The only exception is Mo, which is not separated from S through the AG50-X8 resin. Thus, we conclude that this method is adequate for measuring most common sulfide and sulfate minerals, except Molybdenite.

### *3.4. Laser ablation parameters*

In situ analysis using laser ablation coupled to ICP-MS has been successfully developed and applied for both elemental and isotope ratio measurements of geologic materials (Jackson et al., 1992; Fryer et al., 1995; Horn et al., 2000; Russo et al., 2001; Košler et al., 2005; Mason et al., 2006; Woodhead et al., 2007). To date, most applications have used nanosecond lasers for sample ablation. These are recognized as introducing laser-induced fractionation, which are superimposed on mass fractionation of the ICP-MS. Potential sources of elemental and isotopic fractionation appear to be similar and include, (1) differential evaporation and/or condensation of particles at the site of ablation, (2) variation of particle transport toward the ICP and, (3) incomplete vaporization and ionization of particles in the ICP (Outridge et al., 1997; Eggins et al., 1998; Figg et al., 1998; Horn et al., 2000; Jackson and Günther, 2003; Horn and von

Blanckenburg, 2007). In addition, differences between matrices of the ablated sample and standard aerosols can introduce further mass discrimination and inaccurate mass fractionation correction of ablated samples. In order to obtain the most precise and consistent isotope measurements, it is essential to recognize and minimize mass discrimination introduced by the laser to within the analytical uncertainties achievable by this method. Optimization of laser protocols to minimize laser-induced fractionation has been investigated, and appropriate laser parameters for the determination of S isotopes are presented below.

### *3.4.1. Line scan versus spot ablation*

Experiments were carried out to examine the effect of single spot ('crater') versus line scan ('raster') protocols on isotope fractionation and the precision obtainable by in situ analysis for the anhydrite Sch-M-2 (Figure 6). Laser parameters, including laser optics and pulse energies and frequencies, were kept the same for these comparisons. Line scan ablation results in higher and non-decaying signal intensities, and is reflected in the long-term stability and greater precision of S isotope ratios obtained by this protocol (Figure 6a). For spot mode analysis, signal intensity deteriorates after approximately 90 seconds of ablation. Accordingly, the precision and reproducibility of S isotope compositions using spot analysis diminishes significantly after approximately the same length of time (Figure 6b). Degradation of signal intensity and analytical precision is likely attributable to changes in crater geometry and increasing depth/radius aspect ratio during ablation (Eggins et al., 1998; Horn et al., 2000; Russo et al., 2001). The causes of signal reduction and isotope fractionation related to changes in crater geometry are not precisely known, but may reflect decreasing laser irradiance and increasing thermal conductivity that affect the efficiency of material volatilization and/or condensation, and particle transport at the site of ablation (Eggins et al., 1998; Russo et al., 2001). In raster mode these effects can be largely avoided because the trench depth and geometry remains relatively uniform during ablation, and so differences in particle ablation and particle transport can be minimized. We note that, within analytical uncertainty, Sch-M-2 is isotopically homogenous and does not explain the large variability in isotope ratios measured during spot mode analysis (i.e., no heterogeneity is sampled during depth profiling at a single spot).

Accordingly, line scan analysis is recommended for all in situ isotope measurements where sufficient sample sizes and longer ablation times are available. The internal precision obtainable by line scan mode is typically ± 0.25 ‰ ($1\sigma$). By comparison, the internal precision for spot mode analysis is typically ± 0.5 – 0.6 ‰ ($1\sigma$) for samples ablated for periods of time up to approximately two minutes. Spot mode analysis should be useful for rapid and approximate determination of S isotopes when high precision (≤ 1 ‰) is not required or sample size is severely limited.

### *3.4.2. Carrier gas composition and laser beam diameter*

The effect of varying carrier gas compositions to transport ablated material to the ICP has been investigated extensively previously (Eggins et al., 1998; Günther and Heinrich, 1999b; Jackson and Günther, 2003). Experimental data have indicated that the use of helium, as compared to argon, for the carrier gas significantly increases signal intensities (two- to four-fold increase) and reduces background (Eggins et al., 1998; Günther and Heinrich, 1999a). This observation has been interpreted to reflect, (1) increased evaporation and decreased condensation of ablated particles at the site of ablation and, (2) reduced sputtering of larger particles and increased ionization efficiency of material in the ICP (Eggins et al., 1998; Günther and Heinrich, 1999b). Incomplete vaporization and ionization of large particles in the ICP is a potential cause of isotope fractionation (Jackson and Günther, 2003). Similar effects have been demonstrated for elemental fractionation (Horn et al., 2000). The use of He as a carrier gas has been shown to significantly reduce isotope fractionation (Jackson and Günther, 2003). Accordingly for our study, helium is used as the carrier gas through the laser cell in all instances.

In addition, it has been demonstrated that particle size distribution is dependent on the diameter of the incident beam (Figg et al., 1998; Jeong et al., 1999). Beam optic protocols to minimize the formation of large particles should be adopted, in order to reduce potential isotope fractionation associated with large particles (Jackson and Günther, 2003). The effect of varying beam diameter on particle size distributions has not been examined explicitly because particle filtering apparatus were not available for this study, but have been examined elsewhere (Guillong and Günther, 2002; Jackson and Günther, 2003). Large beam diameters and apertured beam optics will distribute incident laser energy more evenly over the sample surface and may promote the ablation of smaller, more uniformly-sized particles, which will be more efficiently ionized in the ICP. Material ablated with large beam diameters exhibit significantly less mass discrimination during isotope measurement (Horn et al., 2000), likely resulting from more quantitative and equal ionization of all elements and/or isotopes. Similarly for our method, a large beam diameter ~ 60 μm and defocused (apertured) beam optics are recommended for in situ S isotope measurements because these should further minimize laser-induced isotope fractionation.

To validate these laser protocols, replicate sampling and analysis of the anhydrite mineral standard Sch-M-2 was carried out by laser ablation MC-ICP-MS. Measured isotope compositions were compared against data for the same standard analyzed using solution techniques (Figure 7). The isotope composition of Sch-M-2 determined by in situ analysis is $\delta^{34}S_{V\text{-}CDT} = 2.22 \pm 0.45$ ‰ (2σ, 12 replicates). This is identical, within analytical uncertainty, to the isotope composition determined by bulk analysis; $\delta^{34}S_{V\text{-}CDT} = 2.12 \pm 0.26$ ‰ (2σ, 8 replicates). For both mineral and solution analyses, Sch-M-2 was bracketed by a matrix-matched in-house solution standard (see section 3.4.3 for further details). These data indicate that the laser parameters described previously introduce laser isotope fractionations that are within the analytical uncertainties (~ 0.4 ‰) of our in situ S isotope method.

### *3.4.3. Matrix-matching protocols*

The effects of matrix on isotope mass discrimination during in situ S isotope determination are similar to those for bulk analysis. Because it is not possible to remove the complex matrix of natural mineral samples for in situ analysis, it is necessary to assess and correct this matrix fractionation using appropriately matrix-matched standards. Isotopically homogeneous, calibrated and matrix-matched solid standards are not available for many natural mineral samples. Therefore, it may be necessary to use matrix-matched solution standards to bracket unknown mineral samples for in situ analysis. The matrix of solution standards can be readily doped in order to match the wide range of matrix occurring in geologic samples. We have investigated the validity of matrix-matching between solution standards and mineral samples. Replicate analyses of the anhydrite standard Sch-M-2 using conventional solution methods and matrix-matched (Ca-doped) bracketing standards yields an isotope composition $\delta^{34}S_{V\text{-}CDT} = 2.12$

± 0.26 ‰. As presented in Figure 7, this is identical, within analytical uncertainty, to the isotope composition determined by in situ analysis using identical matrix-matched solution standards; $\delta^{34}S_{V\text{-}CDT}$ = 2.22 ± 0.45 ‰. These data are concordant with the S isotope composition obtained previously for Sch-M-2 after chemical purification and analysis as a matrix-free sulfate solution ($\delta^{34}S_{V\text{-}CDT}$ = 2.24 ± 0.27 ‰; Table 3). In contrast, significant and consistent deviations of measured isotope ratios (up to 0.7 ‰) from 'true' isotope ratios are obtained when the Sch-M-2 standard is bracketed by non-matrix-matched standards. These data indicate that, although instrumental mass bias introduced by the complex matrix of mineral samples cannot be removed entirely, it can be appropriately corrected by bracketing with a standard of identical matrix. This is important for obtaining the necessary 'accuracy' of S isotope compositions using this method.

## 4. Application of bulk S-isotope analysis of sulfide and sulfate minerals

### *4.1. S isotope analysis of reference materials*

Because no internationally certified standard reference material is available for S-isotope composition of pure sulfur (i.e. sulfate) solution, it is necessary to use in-house standard solutions to bracket unknown sample solutions across multiple analytical sessions. The $\delta^{34}S$ isotope composition of our in-house standards, $S_{Alfa}$ and $S_{Spex}$, have been calibrated against reference material IAEA-S-1 and have been normalized to the V-CDT scale, assuming by definition an isotope composition of IAEA-S-1 equal to $\delta^{34}S_{V\text{-}CDT}$ = – 0.3 ‰ (Coplen and Krouse, 1998; Ding et al., 2001). Accordingly, the isotope compositions for our in-house standards are $\delta^{34}S_{V\text{-}CDT}$ (Alfa) = + 1.91 ± 0.21 ‰ (2$\sigma$) and $\delta^{34}S_{V\text{-}CDT}$ (Spex) = – 2.99 ± 0.18 ‰ (2$\sigma$). The analysis of S isotope compositions of other RMs (IAEA-S-2, S-4 and NBS-123; Table

3) using our in-house analytes as bracketing standards are concordant with previously reported values within analytical uncertainty (Taylor et al., 2000; Ding et al., 2001; Qi and Coplen, 2003). These data confirm the consistency of our S isotope measurements and the validity of standard-sample bracketing. Reproducibility is typically 0.2 ‰ and is consistent across a wide range of sample material and S-isotope compositions. For example, determination of the S-isotope composition of purified seawater sulfate from Woods Hole, MA (in-house seawater standard) yields a value of $\delta^{34}S_{V\text{-}CDT} = 21.22 \pm 0.19$ ‰ ($2\sigma$), which is undistinguishable within error from the consensus value for modern seawater (Rees et al., 1978). Analysis of S-isotope compositions of both sulfate- and sulfide-bearing reference minerals yielded similar results.The S-isotope compositions determined for the purified in-house standards Sch-M-2 (evaporate anhydrite) and GAV-18 (hydrothermal pyrite) are $\delta^{34}S_{V\text{-}CDT} = 2.27 \pm 0.12$ ‰ and $9.66 \pm 0.2$ ‰, respectively. These isotopic values are within analytical error of S-isotope compositions determined previously using conventional techniques (Table 3).

### *4.1.S isotope analysis of hydrothermal and sedimentary sulfides*

We have analyzed a selection of natural sulfides from sedimentary and hydrothermal environments (Table 4). Sulfur isotope studies provide valuable information for determining sulfur sources and precipitation mechanisms in submarine hydrothermal deposits. Several mechanisms have been proposed to explain variations in the $\delta^{34}S$ values of sulfides in seafloor hydrothermal systems (Janecky and Shanks, 1988; Herzig et al., 1998; Shanks, 2001) and indicate that sulfur has three major sources: (1) sulfur from the leaching of igneous rocks, (2) sulfur from the reduction of a small amount of admixed seawater-derived sulfate, and (3) sulfur produced by disproportionation of magmatic $SO_2$ in back-arc hydrothermal systems. Sulfur isotope results from modern hydrothermal pyrite and chalcopyrite (Table 4) are consistent with previously reported studies (Herzig et al., 1998; Bach et al., 2003; Rouxel et al., 2004). We observe an overall range of $\delta^{34}$S values between – 3.4 to + 6.3 ‰ suggesting that this technique can be used to infer S geochemical cycling in seafloor hydrothermal systems, such as seawater sulfate reduction (increasing S isotope composition) and magmatic S input (producing negative S-isotope composition). In some cases, the difference from published values is significant (up to 0.6 ‰) but may result from sample heterogeneity not identified by bulk analysis.

We have also analyzed a selection of natural sulfides from sedimentary environments (Table 4). Pyrite formation in modern organic-rich marine sediments is mediated by sulfate-reducing bacteria and proceeds through the dissolution and reduction of lithogenic Fe-oxides and silicates to Fe(II), either below the sediment-water interface during diagenesis or in the stratified euxinic bottom waters syngenetically (Canfield, 1989; Anderson and Raiswell, 2004). Hence, S isotope composition of sedimentary pyrite can provide valuable information to distinguish between diagenetic and syngenetic pyrite formation as well as sulfur geochemical cycling in ancient oceans (Zaback et al., 1993; Calvert et al., 1996; Lyons, 1997; Werne et al., 2003; Neretin et al., 2004). Sulfur isotope compositions of pyrite from black shales are also reported in Table 4 and display an overall range of 55 ‰. Small fractionation of S isotopes in late Archean sedimentary sulfides (Jeerinah Formation; Table 4) is consistent with previous studies suggesting sulfate reduction at low sulfate concentrations (Canfield et al., 2000) due to low levels of atmospheric oxygen (Farquhar et al., 2000; Ono et al., 2003). The significant increase in the S isotope fractionation in sedimentary pyrite at 2.32 Ga has been interpreted as reflecting an increase of seawater sulfate concentrations in the aftermath of the rise of atmospheric oxygen (Cameron, 1982; Canfield, 1998; Bekker et al., 2004; Kah et al., 2004). Because this technique is compatible with other non-traditional stable isotope techniques, such as those used for Fe-isotope determination in sedimentary sulfides (Rouxel et al., 2005), it is possible to apply coupled S and Fe stable isotope approaches for the study of ancient S- and Fe- biogeochemical cycling.

## 5. Application of in-situ S isotope analysis of sulfide and sulfate minerals

### *5.1. Assessment of mass fractionation and external reproducibility*

Our instrumental setup for in situ analysis requires no modification to the physical configuration or operating parameters used for bulk solution analysis. Bulk and in situ measurements can be performed interchangeably within a single analytical session. We use the standard-sample bracketing technique for the isotope determination of unknown mineral samples, identical to bulk S isotope measurements. We recognize and caution that the mechanics of particle ablation, aerosol transport and ionization in the ICP are significantly more complex than for solution aspiration. This may result in isotope mass fractionation and accordingly poor analytical precision or inaccurate data. We have presented laser protocols that minimize mass bias introduced by the laser, and which are concordant with results of previous studies (Outridge et al., 1997; Eggins et al., 1998; Figg et al., 1998; Günther and Heinrich, 1999b; Jeong et al., 1999; Horn et al., 2000; Russo et al., 2001; Guillong and Günther, 2002; Jackson and Günther, 2003). Further, differences in the behavior of aerosols for ablated particles as compared to aspirated solutions will contribute to the overall uncertainty of in situ isotope measurement using standard-sample bracketing. Despite these potential difficulties, replicate analysis of the mineral standards indicates relatively precise and consistent isotope ratio determinations as compared to isotope compositions determined by independent bulk analyses (Table 5). The long-term reproducibility of our in situ technique is approximately ± 0.45 ‰ (2σ). Further, the isotope composition of Sch-M-2 determined by bulk ($\delta^{34}S_{V\text{-}CDT} = 2.12 \pm 0.26$ ‰) and in situ ($\delta^{34}S_{V\text{-}CDT} = 2.22 \pm 0.45$ ‰) techniques are identical within these analytical uncertainties, indicating no consistent bias of offset from mass bias corrections using standard-sample bracketing with appropriately matrix-matched standards. This should enable S isotope determinations for a wide range of natural sulfur-bearing samples for which well-characterized, isotopically-homogeneous and appropriately matrix-matched solid standards do not exist.

### *5.2. Future applications of in situ S-isotope analysis of sulfide and sulfate minerals*

Determination of S isotopes using laser-ablation MC-ICP-MS may provide additional information about geochemical and biological processes that might not otherwise be obtained using bulk techniques. A primary application of our in situ analytical routine is to examine S isotope variability in sulfur-bearing hydrothermal and sedimentary materials relevant to the study of sulfide-sulfate deposition in modern and ancient marine environments. In situ analysis is particularly important for systems where significant variations in S isotope compositions may be recorded on small (μm to cm) spatial scales (e.g., within hydrothermal sulfide-sulfate veins or sulfide chimney deposits). In addition, in situ analyses may be necessary for samples for which it is difficult to chemically or physically eliminate matrix from the analyte (e.g., co-existing sulfides or sulfide-sulfate minerals). We have applied our in situ method to the determination of S isotopes in a suite of hydrothermal and sedimentary sulfides and sulfates and can compare our data versus isotope compositions determined using conventional techniques. Overall, the data are in excellent agreement for the range of sulfide and sulfate minerals examined (Table 5). For samples that appear to be isotopically homogeneous based on replicate in situ analyses, our data are the same, within analytical error, to S isotope compositions determined by independent methods. We identify no consistent or significant deviation between S isotope ratios determined by laser ablation MC-ICP-MS and other techniques, which would otherwise indicate some unaccounted mass fractionation by our method. For several sulfide and sulfate, we identify significant isotopic heterogeneity within single samples on spatial scales of mm. These variations are not likely due to matrix artifacts, because in all cases unknown samples are calibrated against matrix-matched standards. Rather, the data likely demonstrate real geochemical heterogeneity recorded by the sample. It is beyond the scope of this paper to discuss the origin of the S isotope variations observed, however our data demonstrate that in situ analytical approaches to S isotope determination can provide information about geochemical processes that might otherwise be overlooked by bulk, conventional techniques.

## 6. Conclusions

We have developed a technique for the rapid, precise and consistent determination of S isotopes ($\delta^{34}S$) by bulk and in situ MC-ICP-MS applicable for a range of sulfur-bearing materials. Major isobaric interferences from molecular $^{16,17,18}O_2^+$ on sulfur masses of interest are removed by applying sufficient mass resolution and determining sulfur intensities on interference free plateaus. Hydride ($^{32}S$-$^{1}H$, $^{33}S$-$^{1}H$) and argon ($^{36}Ar$) interferences are not fully resolved with high mass resolution and limit the application of MC-ICP-MS techniques for accurate multiple S isotope ($\delta^{33}S$, $\delta^{36}S$) determination. We have examined potential contributions to background sulfur signal, including blank contamination and unresolved spectral interferences (e.g., $O_2$-

tailing due to mass drift). Background intensities on sulfur are typically small (30 – 50 mV on $^{32}S$), but may be variable over the course of an analytical session. Average background intensities are determined for each isotope (on-peak zero) and are directly subtracted from the signal intensity for each sulfur isotope as part of off-line evaluation. Approaches to minimize the magnitude of the background correction required to within limits of analytical precision are advantageous because the concentration and isotopic composition of the blank are inherently variable and difficult to characterize. Accordingly, the following procedures are recommended; (1) measure isotope ratios of standard and sample analytes at minimum signal intensities ~ 10 volts and, (2) determine isotope compositions of unknown samples with a standard analyzed at the same intensity (within ~ 20 %). By closely matching signal intensities, the mass bias accounting for effects of instrumental fractionation and background as calculated for the standard, can be appropriately applied to unknown samples.

Instrumental mass bias is corrected by applying the standard-sample bracketing technique, whereby the mass bias calculated for two standard runs immediately before and after are applied by linear interpolation to the unknown sample. We have presented a rigorous examination of matrix effects for S isotope determination by MC-ICP-MS and show that matrix artifacts can produce variable and significant mass bias (up to 0.7 ‰). It is essential that S isotope ratios of samples be determined using appropriately matrix-matched standards. For bulk S isotope analysis, we have described a chemical purification method that is applicable for a wide range of sulfide and sulfate materials whereby the matrix is removed. For in situ analysis, where the matrix cannot be removed prior to analysis, it is essential that appropriately matrix-matched standards be used to correct instrumental mass bias. An important development of our standard-sample bracketing methods is the ability to determine accurate and precise S isotope compositions in *aqueous and mineral samples* with a wide range of matrix, using matrix-matched solution standards in both cases. This has particular application for the in situ analysis of many sulfur-bearing minerals for which certified solid standards with correct matrix do not exist. We have examined sources of isotope fractionation introduced by the laser process. In order to apply the standard-sample bracketing method appropriately using solution standards, it is necessary to minimize laser-induced mass bias to within acceptance limits of uncertainty for the method. Recommended laser protocols are discussed that should enable precise and consistent S isotope ratio measurement by laser ablation MC-ICP-MS.

We have validated the robustness of our analytical method by multiple determinations of reference materials. S isotope ratios for reference materials determined by this study and by independent techniques show excellent agreement demonstrating the 'accuracy' of our method. For solution analysis, the long-term reproducibility of S isotope measurements is typically ± 0.20 ‰ (2σ). For in situ analyis, the external precision calculated by replicate measurement of homogeneous mineral standards is ± 0.45 ‰ (2σ). Importantly, there is good agreement between S isotope ratios for the same standards determined by bulk and in situ analysis (within 0.2 ‰), indicating that standard-sample bracketing can appropriately correct for instrumental mass bias and that laser-induced mass bias is smaller than analytical uncertainties. In addition, we have performed preliminary S isotope determination for a range of natural sulfide and sulfate minerals by laser ablation MC-ICP-MS. Again, the results of this study demonstrate excellent agreement with published data. The analytical technique presented here should enable precise and accurate

S isotope measurement for a wide range of sulfur-bearing materials – in particular for geologic samples with complex matrix for which high-precision, high-resolution in situ analysis is critical.

## Acknowledgements

Support was provided by National Science Foundations grants OCE-0327448 to P.R.C. and W.B. and OCE-0622982 to O.J.R. Support for L.A.B. was provided by the Woods Hole Oceanographic Institution Plasma Facility Development Grant (NSF-EAR/IF-0318137). We thank Andrey Bekker, Yves Fouquet, Volker Lüders, Steven Petsch and David Vanko for access to sample collections. We acknowledge the contributions of two anonymous reviewers and the editor (Roberta Rudnick) who provided detailed and instructive comments and recommendations. These reviews greatly improved the clarity of the manuscript.

## References

Albarède, F. and Beard, B., 2004. Analytical Methods for Non-Traditional Isotopes. Reviews in Mineralogy and Geochemistry, 55: 113-152.

Anbar, A. D. and Rouxel, O. J., 2007. Metal Stable Isotopes in Paleoceanography. Annual Review of Earth and Planetary Sciences, 35(1): 717-746.

Anderson, T. F. and Raiswell, R., 2004. Sources and mechanisms for the enrichment of highly reactive iron in euxinic Black Sea sediments. American Journal of Science, 304: 203-233.

Bach, W., Peucker-Ehrenbrink, B., Hart, S. R. and Blusztajn, J. S., 2003. Geochemistry of hydrothermally altered oceanic crust: DSDP/ODP Hole 504B – Implications for seawater-crust exchange budgets and Sr- and Pb-isotopic evolution of the mantle. Geochemistry Geophysics Geosystems, 4(3): 8904, doi:10.1029/2002GC000419.

Bekker, A., Holland, H. D., Wang, P. L., Rumble, D., Stein, H. J., Hannah, J. L., Coetzee, L. L. and Beukes, N. J., 2004. Dating the rise of atmospheric oxygen. Nature, 427(6970): 117-120.

Belshaw, N. S., Freedman, P. A., O'Nions, R. K., Frank, M. and Guo, Y., 1998. A new variable dispersion double-focusing plasma mass spectrometer with performance illustrated for Pb isotopes. International Journal of Mass Spectrometry, 181: 51–58.

Calvert, S. E., Thode, H. G., Yeung, D. and Karlin, R. E., 1996. A stable isotope study of pyrite formation in the Late Pleistocene and Holocene sediments of the Black Sea. Geochimica et Cosmochimica Acta, 60(7): 1261-1270.

Cameron, E. M., 1982. Sulphate and sulphate reduction in early Precambrian oceans. Nature, 296(5853): 145-148.

Canfield, D. E., 1989. Reactive iron in marine sediments. Geochimica et Cosmochimica Acta, 53: 619-632.

Canfield, D. E., 1998. A new model for Proterozoic ocean chemistry. Nature, 396(6710): 450-453.

Canfield, D. E., 2001. Biogeochemistry of Sulfur Isotopes. Reviews in Mineralogy and Geochemistry, 43: 607-636.

Canfield, D. E., Habicht, K. S. and Thamdrup, B., 2000. The Archean Sulfur Cycle and the Early History of Atmospheric Oxygen. Science, 288(5466): 658-661.

Chaussidon, M., Albarede, F. and Sheppard, S. M. F., 1987. Sulphur isotope heterogeneity in the mantle from ion microprobe measurements of sulphide inclusions in diamonds. Nature, 330(6145): 242-244.

Clough, R., Evans, P., Catterick, T. and Evans, E. H., 2006. $\delta^{34}S$ measurements of sulfur by multicollector inductively coupled plasma mass spectrometry. Analytical Chemistry, 78(17): 6126-6232.

Coplen, T. B. and Krouse, H. R., 1998. Sulphur isotope data consistency improved. Nature, 392(6671): 32.

Ding, T., Valkiers, S., Kipphardt, H., De Bievre, P., Taylor, P. D. P., Gonfiantini, R. and Krouse, R., 2001. Calibrated sulfur isotope abundance ratios of three IAEA sulfur isotope reference materials and V-CDT with a reassessment of the atomic weight of sulfur. Geochimica et Cosmochimica Acta, 65(15): 2433-2437.

Eggins, S. M., Kinsley, L. P. J. and Shelley, J. M. M., 1998. Deposition and element fractionation processes during atmospheric pressure laser sampling for analysis by ICP-MS. Applied Surface Science, 127: 278-286.

Eldridge, C. S., Compston, W., Williams, I. S., Walshe, J. L. and Both, R. A., 1987. In situ microanalysis for $^{34}S/^{32}S$ ratios using the ion microprobe SHRIMP. International Journal of Mass Spectrometry and Ion Processes, 76: 65-83.

Evans, P., Wolff-Briche, C. and Fairman, B., 2001. High accuracy analysis of low level sulfur in diesel fuel by isotope dilution high resolution ICP-MS, using silicon for mass bias correction of natural isotope ratios. Journal of Analytical Atomic Spectrometry, 16: 964-969.

Farquhar, J., Bao, H. and Thiemens, M., 2000. Atmospheric Influence of Earth's Earliest Sulfur Cycle. Science, 289: 756-758.

Faure, G., 1986. Principles of Isotope Geology, 2nd Edition. John Wiley & Sons, New York, 589 pp.

Figg, D. J., Cross, J. B. and Brink, C., 1998. More investigations into elemental fractionation resulting from laser ablation-inductively coupled plasma-mass spectrometry on glass samples. Applied Surface Science, 127-129: 287-291.

Fritz, P., Drimmie, R. J. and Nowicki, V. K., 1974. Preparation of sulfur dioxide for mass spectrometer analyses by combustion of sulfides with copper oxide. Analytical Chemistry, 46(1): 164-166.

Fry, B., Silva, S. R., Kendall, C. and Anderson, R. K., 2002. Oxygen isotope corrections for online $\delta^{34}S$ analysis. Rapid Communications in Mass Spectrometry, 16(9): 854-858.

Fryer, B. J., Jackson, S. E. and Longerich, H. P., 1995. The design, operation and role of the laser-ablation microprobe coupled with an inductively coupled plasma mass spectrometer (LAM-ICP-MS) in the Earth sciences. The Canadian Mineralogist, 33: 303-312.

Galy, A., Pomies, C., Day, J. A., Pokrovsky, O. S. and Schott, J., 2003. High precision measurement of germanium isotope ratio variations by multiple collector-inductively coupled plasma mass spectrometry. Journal of Analytical Atomic Spectrometry, 18: 115-119.

Giesemann, A., Jaeger, H. J., Norman, A. L., Krouse, H. R. and Brand, W. A., 1994. Online Sulfur-Isotope Determination Using an Elemental Analyzer Coupled to a Mass Spectrometer. Analytical Chemistry, 66(18): 2816-2819.

Goldhaber, M. B. and Kaplan, I. R., 1974. The sulphur cycle. In: E. D. Goldberg (Editor), The Sea, pp. 569–655.

Grassineau, N. V., Mattey, D. P. and Lowry, D., 2001. Sulfur Isotope Analysis of Sulfide and Sulfate Minerals by Continuous Flow-Isotope Ratio Mass Spectrometry. Analytical Chemistry, 73: 220-225.

Günther, D. and Heinrich, C. A., 1999a. Comparison of the ablation behaviour of 266nm Nd:YAG and 193 nm ArF excimer lasers for LA-ICP-MS analysis. Journal of Analytical Atomic Spectrometry, 14: 1369-1374.

Günther, D. and Heinrich, C. A., 1999b. Enhanced sensitivity in laser ablation-ICP mass spectrometry using helium-argon mixtures as aerosol carrier. Journal of Analytical Atomic Spectrometry, 14: 1363-1368.

Guillong, M. and Günther, D., 2002. Effect of particle size distribution on ICP-induced elemental fractionation in laser ablation-inductively coupled plasma-mass spectrometry. Journal of Analytical Atomic Spectrometry, 17: 831-837.

Halliday, A. N., Lee, D. C., Christensen, J. N., Rehkamper, M., Yi, W., Luo, X., Hall, C. M., Ballentine, C. J., Pettke, T. and Stirling, C., 1998. Applications of multiple collector-

ICPMS to cosmochemistry, geochemistry and paleoceanography. Geochimica et Cosmochimica Acta, 62(6): 919-940.

Herzig, P. M., Hannington, M. D. and Arribas, A., Jr., 1998. Sulfur isotopic composition of hydrothermal precipitates from the Lau back-arc: implications for magmatic contributions to seafloor hydrothermal systems. Mineralium Deposita, 33(3): 226-237.

Hoefs, J., 1997. Stable Isotope Geochemistry, 4th Edition. Springer, New York, 201 pp.

Horn, I., Rudnick, R. L. and McDonough, W. F., 2000. Precise elemental and isotope ratio determination by simultaneous solution nebulization and laser ablation-ICP-MS: application to U-Pb geochronology. Chemical Geology, 164(3): 281-301.

Horn, I. and von Blanckenburg, F., 2007. Investigation on elemental and isotopic fractionation during 196 nm femtosecond laser ablation multiple collector inductively coupled plasma mass spectrometry. Spectrochimica Acta Part B: Atomic Spectroscopy, 62: 410-422.

Hu, G., Rumble, D., III and Wang, P., 2003. An ultraviolet laser microprobe for the in situ analysis of multisulfur isotopes and its use in measuring Archean sulfur isotope mass-independent anomalies. Geochimica et Cosmochimica Acta, 67(17): 3101-3118.

Jackson, S. E. and Günther, D., 2003. The nature and sources of laser induced isotopic fractionation in laser ablation-multicollector-inductively coupled plasma-mass spectrometry. Journal of Analytical Atomic Spectrometry, 18: 205-212.

Jackson, S. E., Longerich, H. P., Dunning, G. R. and Freyer, B. J., 1992. The application of laser-ablation microprobe inductively coupled plasma-mass spectrometry (LAM-ICP-MS) to in situ trace-element determinations in minerals. The Canadian Mineralogist, 30: 1049-1064.

Janecky, D. R. and Shanks, W. C., III, 1988. Computational modeling of chemical and sulfur isotopic reaction processes in seafloor hydrothermal systems: chimneys, massive sulfides, and subjacent alteration zones. Canadian Mineralogist, 26: 805-825.

Jarvis, K. E., Gray, A. L. and Houk, R. S., 1992. Handbook of Inductively Coupled Plasma Mass Spectrometry. Blackie, Glasgow, United Kingdom.

Jeong, S. H., Borisov, O. V., Yoo, J. H., Mao, X. L. and Russo, R. E., 1999. Effects of particle size distribution on inductively coupled plasma mass spectrometry signal intensity during laser ablation of glass samples. Analytical Chemistry, 71(22): 5123-5130.

Kah, L. C., Lyons, T. W. and Frank, T. D., 2004. Low marine sulphate and protracted oxygenation of the Proterozoic biosphere. Nature, 431: 834-838.

Košler, J., Pedersen, R. B., Kruber, C. and Sylvester, P. J., 2005. Analysis of Fe isotopes in sulfides and iron meteorites by laser ablation high-mass resolution multi-collector ICP mass spectrometry. Journal of Analytical Atomic Spectrometry, 20(3): 192-199.

Krupp, E. M., Pécheyran, C., Meffan-Main, S. and Donard, O. F. X., 2004. Precise isotope-ratio determination by CGC hyphenated to ICP–MCMS for speciation of trace amounts of gaseous sulfur, with SF6 as example compound. Analytical and Bioanalytical Chemistry, 378(2): 250-255.

Lyons, T. W., 1997. Sulfur isotopic trends and pathways of iron sulfide formation in upper Holocene sediments of the anoxic Black Sea. Geochimica et Cosmochimica Acta, 61(16): 3367-3382.

Mann, J. L. and Kelly, W. R., 2005. Measurement of sulfur isotope composition ($\delta^{34}S$) by multiple-collector thermal ionization mass spectrometry using a $^{33}S$-$^{36}S$ double spike. Rapid Communications in Mass Spectrometry, 19: 3429-3441.

Maréchal, C. N., Télouk, P. and Albarède, F., 1999. Precise analysis of copper and zinc isotopic compositions by plasma-source mass spectrometry. Chemical Geology, 156(1-4): 251-273.

Mason, P. R. D., Kaspers, K. and van Bergen, M. J., 1999. Determination of sulfur isotope ratios and concentrations in water samples using ICP-MS incorporating hexapole ion optics. Journal of Analytical Atomic Spectrometry, 14: 1067-1074.

Mason, P. R. D., Kosler, J., de Hoog, J. C. M., Sylvester, P. J. and Meffan-Main, S., 2006. In situ determination of sulfur isotopes in sulfur-rich materials by laser ablation multiple-collector inductively coupled plasma mass spectrometry (LA-MC-ICP-MS). Journal of Analytical Atomic Spectrometry, 21: 177-186.

Menegário, A. A., Giné, M. F., Bendassolli, J. A., Bellato, A. C. S. and Trivelin, P. C. O., 1998. Sulfur isotope ratio ($^{34}S$:$^{32}S$) measurements in plant material by inductively coupled plasma mass spectrometry. Journal of Analytical Atomic Spectrometry, 13: 1065-1067.

Mojzsis, S. J., Coath, C. D., Greenwood, J. P., McKeegan, K. D. and Harrison, T. M., 2003. Mass-independent isotope effects in Archean (2.5 to 3.8 Ga) sedimentary sulfides determined by ion microprobe analysis. Geochimica et Cosmochimica Acta, 67(9): 1635-1658.

Neretin, L. N., Boettcher, M. E., Joergensen, B. B., Volkov, II, Lueschen, H. and Hilgenfeldt, K., 2004. Pyritization processes and greigite formation in the advancing sulfidization front in the upper Pleistocene sediments of the Black Sea. Geochimica et Cosmochimica Acta, 68(9): 2081-2093.

Ohmoto, H. and Rye, R. O., 1979. Isotopes of sulfur and carbon. In: H. L. Barnes (Editor), Geochemistry of Hydrothermal Ore Deposits, 2nd Edition. Wiley-Interscience, pp. 509-567.

Ono, S., Eigenbrode, J. L., Pavlov, A. A., Kharecha, P., Rumble, D., III, Kasting, J. F. and Freeman, K. H., 2003. New insights into Archean sulfur cycle from mass-independent sulfur isotope records from the Hamersley Basin, Australia. Earth and Planetary Science Letters, 213(15): 15-30.

Outridge, P. M., Doherty, W. and Gregoire, D. C., 1997. Ablative and transport fractionation of trace elements during laser sampling of glass and copper. Spectrochimica Acta Part B: Atomic Spectroscopy, 52: 2093-2102.

Paterson, B. A., Riciputi, L. R. and McSween, H. Y., 1997. A comparison of sulfur isotope ratio measurement using two ion microprobe techniques and application to analysis of troilite in ordinary chondrites. Geochimica et Cosmochimica Acta, 61(3): 601-609.

Pietruszka, A. J., Walker, R. J. and Candela, P. A., 2006. Determination of mass-dependent molybdenum isotopic variations by MC-ICP-MS: An evaluation of matrix effects. Chemical Geology, 225(1-2): 121-136.

Prohaska, T., Latkoczy, C. and Stingeder, G., 1999. Precise sulfur isotope ratio measurements in trace concentration of sulfur by inductively coupled plasma double focusing sector field mass spectrometry. Journal of Analytical Atomic Spectrometry, 14: 1501-1504.

Qi, H. P. and Coplen, T. B., 2003. Evaluation of the $^{34}S/^{32}S$ ratio of Soufre de Lacq elemental sulfur isotopic reference material by continuous flow isotope-ratio mass spectrometry. Chemical Geology, 199(1): 183-187.

Rees, C. E., 1978. Sulphur isotope measurements using $SO_2$ and $SF_6$. Geochimica et Cosmochimica Acta, 42: 383-389.

Rees, C. E., Jenkins, W. J. and Monster, J., 1978. The sulphur isotopic composition of ocean water sulphate. Geochimica et Cosmochimica Acta, 42(4): 377-381.

Rehkämper, M. and Halliday, A. N., 1998. Accuracy and long-term reproducibility of lead isotopic measurements by MC-ICP-MS using an external method for correction of mass discrimination. International Journal of Mass Spectrometry and Ion Processes, 58: 123–133.

Riciputi, L. R., Paterson, B. A. and Ripperdan, R. L., 1998. Measurement of light stable isotope ratios by SIMS: Matrix effects for oxygen, carbon, and sulfur isotopes in minerals. International Journal of Mass Spectrometry, 178(1): 81-112.

Robinson, B. W. and Kusakabe, M., 1975. Quantitative preparation of sulfur dioxide, for sulfur-34/sulfur-32 analyses, from sulfides by combustion with cuprous oxide. Analytical Chemistry, 47(7): 1179-1181.

Rouxel, O. J., Bekker, A. and Edwards, K. J., 2005. Iron Isotope Constraints on the Archean and Paleoproterozoic Ocean Redox State. Science, 307: 1088-1091.

Rouxel, O. J., Fouquet, Y. and Ludden, J. N., 2004. Subsurface processes at the Lucky Strike hydrothermal field, Mid-Atlantic ridge: Evidence from sulfur, selenium, and iron isotopes. Geochimica et Cosmochimica Acta, 68: 2295-2311.

Russo, R. E., Mao, X., Liu, H., Gonzalez, J. and S., M. S., 2001. Laser ablation in analytical chemistry - A review. Paper LBNL-48521, Lawrence Berkeley National Laboratory.

Shanks, W. C., III, 2001. Stable Isotopes in Seafloor Hydrothermal Systems: Vent fluids, hydrothermal deposits, hydrothermal alteration and microbial processs. Reviews in Mineralogy and Geochemistry, 43: 469-525.

Shanks, W. C., III, Crowe, D. E. and Johnson, C., 1998. Sulfur isotope analyses using the laser microprobe. In: M. A. McKibben, W. C. Shanks, III and W. I. Ridley (Editors), Applications of Microanalytical Techniques to Understanding Mineralizing Processes. Reviews in Economic Geology. Society of Economic Geologists, pp. 141-153.

Studley, S. A., Ripley, E. M., Elswick, E. R., Dorais, M. J., Fong, J., Finkelstein, D. and Pratt, L. M., 2002. Analysis of sulfides in whole rock matrices by elemental analyzer-continuous flow isotope ratio mass spectrometry. Chemical Geology, 192(1): 141-148.

Tanner, S. D., 1992. Space charge in ICP-MS: calculation and implications. Spectrochimica Acta Part B: Atomic Spectroscopy, 47: 809-823.

Taylor, B. E., Ding, T., Halas, S., Breas, O. and Robinson, B. W., 2000. Accurate calibration of the V-CDT Scale: proposed $\delta^{34}S$ values for calibration and reference materials and methods of correction for $SO_2$-based analyses. Report of Sulfur Isotope Working Group 8th Advisory Group Meeting on Future Trends in Stable Isotope Reference Materials and Laboratory Quality Assurance, IAEA, Vienna, Austria.

Thode, H. G., Monster, J. and Dunford, H. B., 1961. Sulphur isotope geochemistry. Geochimica et Cosmochimica Acta, 25: 159-174.

Vanhaecke, F., Dams, R. and Vandecasteele, C., 1993. Zone model as an explanation for signal behaviour and non-spectral interferences in inductively coupled plasma mass spectrometry. Journal of Analytical Atomic Spectrometry, 8: 433-438.

Werne, J. P., Lyons, T. W., Hollander, D. J., Formolo, M. J. and Sinninghe Damste, J. S., 2003. Reduced sulfur in euxinic sediments of the Cariaco Basin: sulfur isotope constraints on organic sulfur formation. Chemical Geology, 195(1-4): 159-179.

Weyer, S. and Schwieters, J. B., 2003. High precision Fe isotope measurements with high mass resolution MC-ICPMS. International Journal of Mass Spectrometry, 226(3): 355-368.

Woodhead, J. D., Hellstrom, J., Hergt, J. M., Greig, A. and Maas, R., 2007. Isotopic and Elemental Imaging of Geological Materials by Laser Ablation Inductively Coupled Plasma-Mass Spectrometry. Geostandards and Geoanalytical Research, 31(4): 331-343.

You, C.-F. and Li, M.-D., 2005. Precise determination of sulfur isotopic ratio in aqueous solutions by inductively coupled plasma mass spectrometry. Journal of Analytical Atomic Spectrometry, 20: 1392-1394.

Zaback, D. A., Pratt, L. M. and Hayes, J. M., 1993. Transport and reduction of sulfate and immobilization of sulfide in marine black shales. Geology, 21(2): 141-144.

**Figure Captions**

Figure 1.

Schematic diagram of the introduction system to the NEPTUNE MC-ICP-MS. Standard and sample solutions are taken up in Ar gas flow and introduced as a 'wet' aerosol (in 2% $HNO_3$) into the ICP torch via a cyclonic spray dual chamber. During in situ analysis, ablated material is carried via He gas flow into the cyclonic spray dual chamber where it is mixed with ultra-pure 2% $HNO_3$ to yield a wet aerosol.

Figure 2.

Peak shapes for S-isotopes at masses 32 (diamond), 33 (square) and 34 (triangle) for aspiration of a 20 ppm S solution. Beams are collected simultaneously on three individual Faraday Cups in 'high-resolution' mode. Significant interferences from $O_2^+$ occur on all sulfur masses (light-gray bar) and must be removed using sufficient mass resolution to enable detection of S-isotopes on the interference-free plateau at lower mass (dark-gray bar).

Figure 3.

Variability of measured $^{34}S/^{32}S$ isotope ratio as a function of $^{32}S$ signal intensity for $S_{Alfa}$ standard solution. For signal intensities below 1 volt (equivalent to ~ 2 ppm S) mass bias toward heavy $^{34}S/^{32}S$ ratios is significant resulting from blank artifacts (highlighted gray area) that require appropriate correction.

Figure 4.

Long-term reproducibility of S-isotope for in-house solution standards $S_{Alfa}$ and $S_{Spex}$ calibrated against certified standards over multiple, independent analytical sessions. Data are shown relative to the in-house $S_{Spex}$ scale. For $\delta^{34}S$ values, the reproducibility is within ± 0.2 ‰ for both solutions. For $\delta^{33}S$, the reproducibility is poor because of variable and significant interference on mass 33 from formation of $^{32}S$-$^{1}H$ hydride.

Figure 5.

Assessment of matrix effects on measured S-isotope ratios for a range of elements with stoichiometry appropriate to various sulfide and sulfate minerals (shown with open circles). Element-doped S solutions are measured and isotopic compositions are expressed as permil deviation on the V-CDT scale from the composition determined for the pure S (i.e., sulfate) standard ($\Delta^{34}S = \delta^{34}S_{(matrix\ solution)} - \delta\ ^{34}S_{(pure\ S\ solution)}$). The element-doped solutions were purified and the isotope composition re-determined (filled diamonds). Following purification, the deviation between the pure S standard and purified solutions is within analytical uncertainty. External precision calculated at ± 0.2 ‰ is shown by the gray bar.

Figure 6.

Signal intensities and measured isotope ratios for anhydrite standard Sch-M-2 using (a) line scan (‘raster’) ablation and (b) single spot ablation. ICP-MS operating parameters were identical for acquisition of both data. Signal intensities for line scan ablation are significantly higher as compared to spot ablation and remain high throughout the ablation period. Accordingly, $^{34}S/^{32}S$ isotope ratios determined for line scan analysis are more precise and consistent with isotope ratios for Sch-M-2 determined using conventional bulk techniques (shown by horizontal gray bar; $\delta^{34}S = 2.27 \pm 0.24$ ‰, 2σ). The oscillating fluctuation of signal intensity for line scan mode arises because the mass of material ablated material varies as extra laser pulses are applied to a single area during changes of the direction of sample movement in line scan analysis. This artifact does not compromise the precision obtainable by in situ analysis at these high signal intensities.

Figure 7.

Comparison of S isotope compositions determined for the in-house anhydrite standard Sch-M-2 using *bulk* analysis (gray diamonds) and in situ analysis (gray circles). In both cases, the isotope value composition of anhydrite was calibrated against a matrix-matched (Ca-doped) sulfur standard, $S_{Alfa}$. The isotopic compositions determined for Sch-M-2 are identical within analytical uncertainties for both methods using matrix-matching procedures. Significant mass bias offset is observed for Sch-M-2 when calibrated against a non-matrix-matched $S_{Alfa}$ standard, resulting in erroneous S isotope determinations (white diamonds). Error bars for single analyses are 1σ (internal precision). Mean isotope compositions calculated from replicate analyses are reported at 2σ (external precision).

**Table 1** Typical operating parameters for NEPTUNE MC-ICPMS and NewWave UP213 laser.

| | |
|---|---|
| *Mass Spectrometer Setup* | |
| MC-ICP-MS | ThermoElectron NEPTUNE |
| RF power | ~ 1150 W |
| Pt-guard electrode | On, grounded |
| Gas flows | |
| Cooling gas | ~ 15 L/min, Ar |
| Auxiliary gas | ~ 0.8 L/min, Ar |
| Sample gas | ~ 0.8 - 0.9 L/min, Ar |
| Laser "carrier" gas | ~ 0.35 - 0.4 L/min, He |
| Interface cones | X-cones (Ni) |
| Analyzer pressure | ~ $10^{-9}$ torr |
| Nebulizer | PFA-50, Elemental Scientific, Inc. |
| Sample uptake rate | 50 µL/min |
| Spray Chamber | SSI cyclonic spray dual chamber, Elemental Scientific, Inc. |
| | |
| *Data Acquisition Parameters* | |
| Acquisition mode | Static, analogue detectors |
| Detection system | Faraday cups |
| Cup configuration | $^{32}$S (L3), $^{33}$S (C), $^{34}$S (H3) |
| Resolution mode | High (entrance slit); Low (detector slit) |
| Signal analysis protocol | 8.5 sec integration per cycle, 20 cycles. |
| Wash-out time | 2 min (solution); 4 min (laser) |
| | |
| *Laser Setup* | |
| Laser | New Wave UP213, (quad Nd:YAG 213 nm laser) |
| Carrier gas | Helium |
| Beam optics | Apertured Mode |
| Spot diameter | 60 µm |
| Raster protocols | Pattern area 180 x 80 µm, Line spacing 15 µm |
| Scan speed | 5 µm/s |
| Ablation duration (analysis time) | 260 s |
| Pulse rate | 10 Hz |
| Laser intensity | 50 - 70 % (~ 0.4 mJ) |
| Energy density | ~ 9 - 10 J/cm$^2$ |
| Pre-ablation | same raster and spot size, scan speed 30 µm/s, intensity 40 % |

**Table 2** Isobaric (spectral) interferences on sulfur isotope masses

| Isotope | Abundance (%) | Interference | Abundance | m/Δm |
|---|---|---|---|---|
| $^{32}S$ | 94.93 | $^{16}O$-$^{16}O$ | 99.52 | 1801 |
| | | $^{64}Zn^{2+}$ | 48.89 | -4562 |
| | | $^{15}N$-$^{16}O$-$^{1}H$ | 0.37 | 1040 |
| $^{33}S$ | 0.76 | $^{17}O$-$^{16}O$ | 0.08 | 1461 |
| | | $^{16}O$-$^{16}O$-$^{1}H$ | 99.51 | 1260 |
| | | $^{32}S$-$^{1}H$ | 95.01 | 3907 |
| | | $^{66}Zn^{2+}$ | 27.81 | -3905 |
| $^{34}S$ | 4.29 | $^{18}O$-$^{16}O$ | 0.4 | 1297 |
| | | $^{17}O$-$^{16}O$-$^{1}H$ | 0.76 | 1000 |
| | | $^{33}S$-$^{1}H$ | 0.75 | 2977 |
| | | $^{68}Zn^{2+}$ | 18.56 | -6238 |
| $^{36}S$ | 0.02 | $^{36}Ar$ | 0.34 | 77083 |
| | | $^{35}Cl$-$^{1}H$ | 75.76 | 3747 |

**Table 3** Reference materials and standards determined by this study

| Name | Sample Type | # of replicates | $\delta^{34}$S Spex | 2$\sigma^{\$}$ | $\delta^{34}$S VCDT | 2$\sigma^{\xi}$ | $\delta^{34}$S VCDT * |
|---|---|---|---|---|---|---|---|
| ***Reference Materials*** | | | | | | | |
| **IAEA-S-1** | **Synthetic $Ag_2S$** | **13** | **2.69** | 0.21 | **-0.30** | 0.28 | **-0.30 (a,b)** |
| **IAEA-S-2** | **Synthetic $Ag_2S$** | **11** | **25.43** | 0.39 | **22.44** | 0.43 | **22.67 ± 0.26 (c)** |
| **IAEA-S-4** | **Elemental S** | **10** | **19.54** | 0.22 | **16.55** | 0.29 | **16.9 ± 0.2 (e)** |
| **NBS-123** | **Natural ZnS** | **11** | **20.76** | 0.19 | **17.77** | 0.26 | **17.44 ± 0.2 (c,d)** |
| ***In-house Standards*** | | | | | | | |
| **Alfa** | **Specpure $SO_4^{2-}$ solution** | **20** | **4.90** | 0.24 | **1.91** | 0.30 | **n.d.** |
| **Sch-M-2** | **Permian Anhydrite, $CaSO_4$** | **8** | **5.23** | 0.20 | **2.24** | 0.27 | **2.49 ± 0.2** |
| **SW-Woods Hole** | **Modern Seawater, Woods Hole** | **4** | **24.18** | 0.19 | **21.19** | 0.27 | **20.99 (f)** |
| **FeIII-sulfate** | **Synthetic $Fe_2SO_4.3H_2O$** | **6** | **11.33** | 0.14 | **8.34** | 0.23 | **n.d.** |
| **GAV-18** | **Hydrothermal pyrite, $FeS_2$** | **8** | **12.61** | 0.19 | **9.62** | 0.27 | **9.70** |
| **Ward's Py** | **Hydrothermal pyrite, $FeS_2$** | **7** | **5.56** | 0.28 | **2.57** | 0.33 | **n.d.** |
| **Ward's Po** | **Hydrothermal pyrrhotite, FeS** | **3** | **3.67** | 0.17 | **0.68** | 0.25 | **n.d.** |

---

[\$] External precision (two standard deviations) calculated from replicate analyses

[ξ] External precision calculated (two standard deviations) using error propagation of uncertainties of sample and bracketing standard. i.e., $2\sigma = \sqrt{((2\sigma \text{ of sample})^2 + (2\sigma \text{ of Spex standard})^2)}$

* published data, errors given at 2σ uncertainty: (a) Coplen and Krouse, 1998; (b) Ding et al., 2001; (c) Taylor et al., 2000; (d) Hut, 1987; (e) Qi and Coplen, 2003; (f) Rees et al., 1978

**Table 4** Bulk analysis of representative natural sulfides from hydrothermal and sedimentary environments

| Name | Sample Type | $\delta^{34}$S Spex | 1σ[$] | $\delta^{34}$S VCDT | 1σ[$] | $\delta^{34}$S VCDT * |
|---|---|---|---|---|---|---|
| ***Modern Hydrothermal Sulfides*** | | | | | | |
| MS-18-05 cpy | chalcopyrite | **8.32** | 0.11 | **5.33** | 0.21 | **5.0 (a)** |
| MS-21-03 cpy | chalcopyrite | **9.32** | 0.13 | **6.33** | 0.22 | **5.6 (a)** |
| NL-16-02 cpy | chalcopyrite | **-0.36** | 0.11 | **-3.35** | 0.21 | **-3.4 (b)** |
| 83-504B-80R1,62 | pyrite | **6.57** | 0.27 | **3.58** | 0.32 | **3.5 (c)** |
| 83-504B-84R2,34 | pyrite | **6.75** | 0.27 | **3.76** | 0.32 | **4.0 (c)** |
| ***Kentucky Black Shales, Clay City (Devonian)*** | | | | | | |
| Clay City. 510-519 #2 | pyrite | **-16.81** | 0.49 | **-19.80** | 0.52 | **(d)** |
| ClayCity, 193-200 Leach | pyrite | **-18.53** | 0.09 | **-21.52** | 0.20 | |
| ClayCity, 232-238 Leach) | pyrite | **-21.18** | 0.08 | **-24.17** | 0.20 | |
| ***Black Shales, Illinois Basin (Devonian)*** | | | | | | |
| SH-Dev-1 #1 | pyrite | **26.17** | 0.19 | **23.18** | 0.26 | **(d)** |
| SH-Dev-2 #1 | pyrite | **-0.68** | 0.20 | **-3.67** | 0.27 | |
| SH-Dev-3 #1 | pyrite | **-7.99** | 0.14 | **-10.98** | 0.23 | |
| SH-Dev-3 #2 | pyrite | **-8.28** | 0.16 | **-11.27** | 0.24 | |
| SH-Dev-3 #3 | pyrite | **-7.63** | 0.23 | **-10.62** | 0.30 | |
| ***2.32 Ga Rooihoogte and Timeball Hill Formations, Transvaal Basin, South Africa*** | | | | | | |
| EBA-2/55 | pyrite | **-25.17** | 0.07 | **-28.16** | 0.19 | **-29.1; -29.6 (e)** |
| EBA-2/59 | pyrite | **-23.96** | 0.08 | **-26.95** | 0.20 | **-25.6; -28.8 (e)** |
| EBA-2/60 | pyrite | **-28.97** | 0.00 | **-31.96** | 0.18 | **-28.9; -30.0 (e)** |
| EBA-2/67 | pyrite | **-25.67** | 0.27 | **-28.66** | 0.32 | **-23.9; -29.9 (e)** |
| ***2.63 Ga Royal Hill Member of the Jeerinah Formation, Hamersley Basin, Western Australia*** | | | | | | |
| FVG-1, 722.6 | pyrite | **6.10** | 0.10 | **3.11** | 0.21 | **-0.4 to 6.3 (f)** |
| FVG-1, 752.8 | pyrite | **5.85** | 0.11 | **2.86** | 0.21 | |
| FVG-1, 761.8 | pyrite | **7.92** | 0.00 | **4.93** | 0.18 | |
| FVG-1, 787.4 | pyrite | **5.53** | 0.04 | **2.54** | 0.18 | |
| FVG-1, 849.6 | pyrite | **1.07** | 0.04 | **-1.92** | 0.18 | |

---

[$] Internal precision (one standard deviation) for individual measurement.

* Published data (a) Rouxel et al., 2004; (b) Herzig et al., 1998; (c) Bach et al., 2003; (d) A. Bekker, *pers. comm.* (e) Bekker et al., 2004; (f) Ono et al., 2003

**Table 5** In situ sulfur isotope analysis of natural sulfides and sulfates from hydrothermal and sedimentary environments

| Name | | Sample Type | **$\delta^{34}$S Spex** | **$\delta^{34}$S VCDT[ξ]** | **$\delta^{34}$S VCDT[$]** |
|---|---|---|---|---|---|
| ***Hydrothermal Sulfides*** | | | | | |
| *ALV-4053-M1 #A1* | | marcasite | | | **2.0 ± 0.2 (a)** |
| | raster #1 | | **5.21** | **2.21** | |
| | raster #2 | | **5.31** | **2.31** | |
| | raster #3 | | **5.14** | **2.14** | |
| GAV-18 | | pyrite | | | **9.7 ± 0.2 (b)** |
| | raster #1 | | **12.83** | **9.84** | |
| | raster #2 | | **12.93** | **9.94** | |
| | raster #3 | | **13.38** | **10.39** | |
| FL-19-9 | | pyrite | | | **0 ± 0.2 (c)** |
| | raster #1 | | **2.77** | **-0.22** | |
| | raster #2 | | **3.35** | **0.36** | |
| | raster #3 | | **3.54** | **0.55** | |
| | raster #4 | | **3.51** | **0.52** | |
| ***2.32 Ga Rooihoogte and Timeball Hill formations, Transvaal Basin, South Africa*** | | | | | |
| EBA-2/30 | | pyrite | | | **-25.6; -26.2 (d)** |
| | raster #1 | | **-26.21** | **-29.21** | |
| | raster #2 | | **-25.83** | **-28.83** | |
| | raster #3 | | **-25.49** | **-28.49** | |
| | raster #4 | | **-25.62** | **-28.62** | |
| | raster #5 | | **-24.85** | **-27.85** | |
| | raster #6 | | **-25.40** | **-28.40** | |
| | raster #7 | | **-24.95** | **-27.95** | |
| | raster #8 | | **-19.87** | **-22.87** | |
| | raster #9 | | **-19.47** | **-22.47** | |
| | raster #10 | | **-20.46** | **-23.46** | |
| | raster #11 | | **-21.83** | **-24.83** | |
| ***Hydrothermal Sulfates*** | | | | | |
| 193-1188A-7R-1 | | anhydrite | | | **21.6 (e)** |
| | raster #1 | | | **21.22** | |
| | raster #2 | | | **21.22** | |
| | raster #3 | | | **21.13** | |
| | raster #4 | | | **21.07** | |
| 193-1188F-26Z-1 | | anhydrite | | | **18.3 (e)** |
| | raster #1 | | | **16.61** | |
| | raster #2 | | | **17.43** | |
| | raster #3 | | | **18.55** | |
| | raster #4 | | | **18.00** | |
| | raster #5 | | | **19.01** | |
| | raster #6 | | | **18.65** | |

[ξ] Normalized to V-CDT scale using $\delta^{34}$S of in-house Spex vs. V-CDT = - 2.99 ‰

[$] Determined using conventional, bulk analysis; (a) Rouxel et al., 2007; (b) Rouxel, *unpubl.,* this study; (c) Rouxel et al., 2004; (d) Bekker et al., 2004; (e) Bach et al., 2005

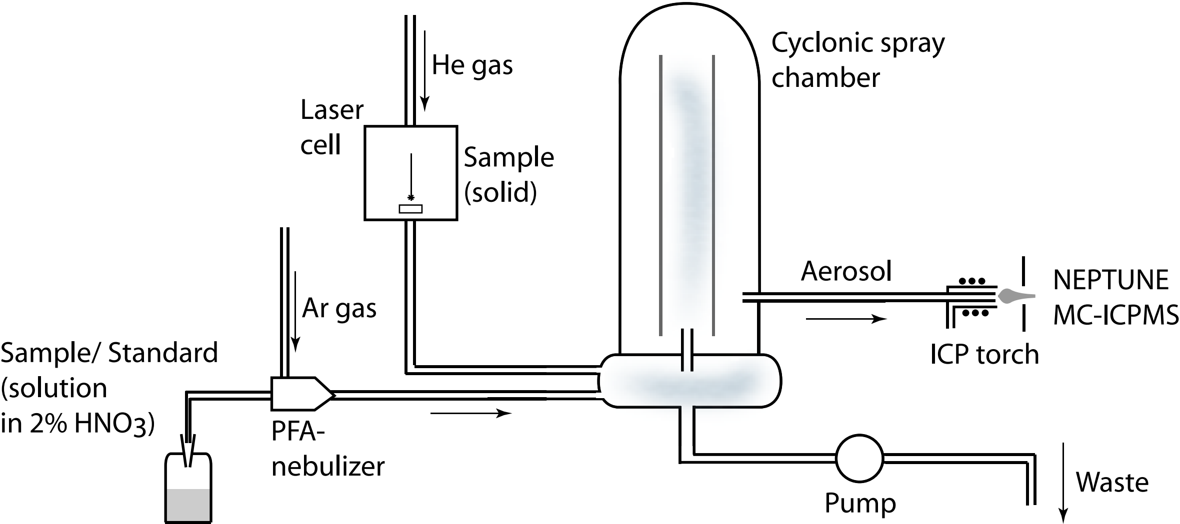
He gas
Laser
cell
Sample
(solid)
Cyclonic spray
chamber
Ar gas
Aerosol
NEPTUNE
MC-ICPMS
ICP torch
Sample/ Standard
(solution
in 2% HNO3)
PFA-
nebulizer
Pump
Waste

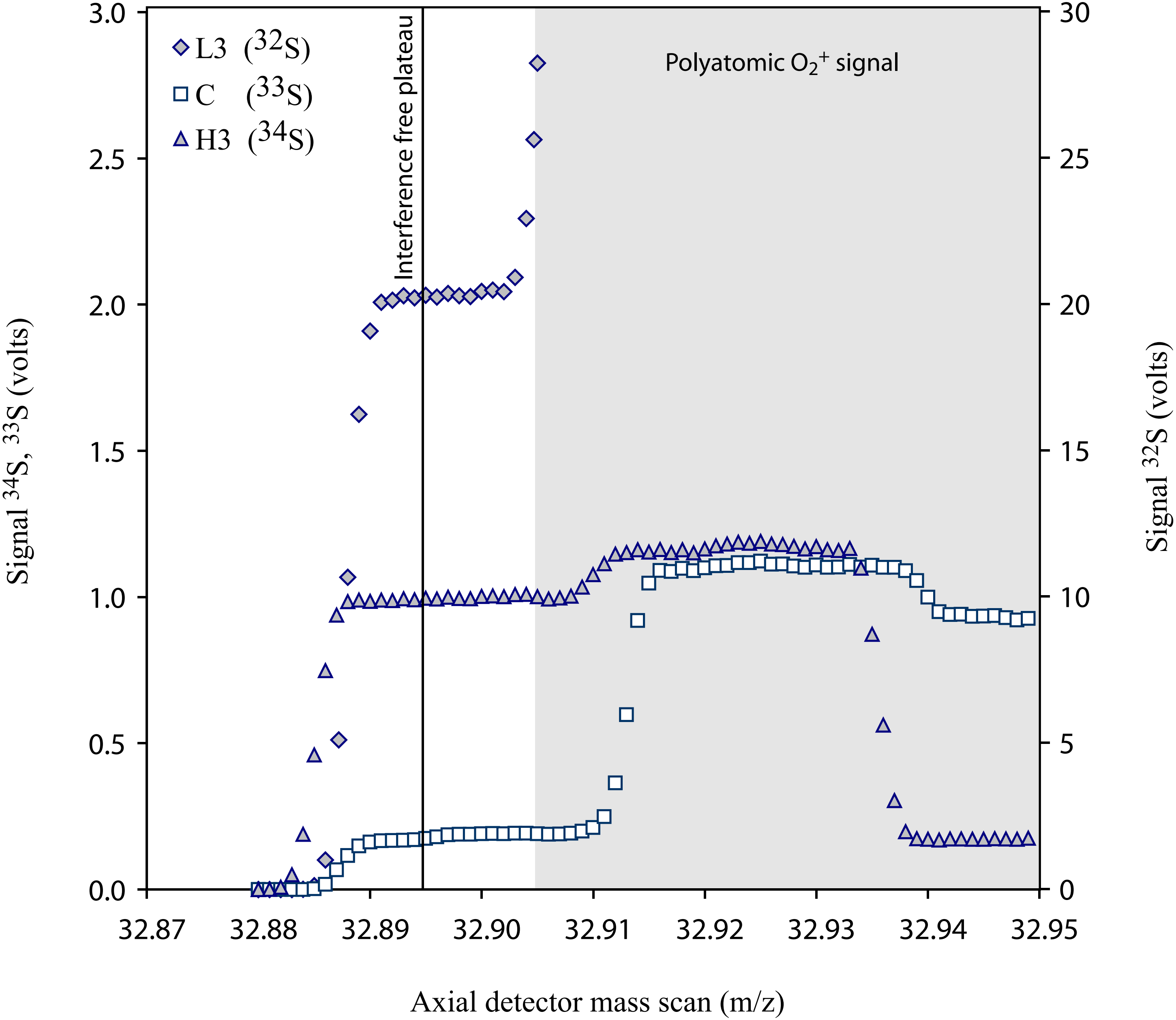
L3 ($^{32}$S)
C ($^{33}$S)
H3 ($^{34}$S)
Interference free plateau
Polyatomic $O_2^+$ signal
Signal $^{34}$S, $^{33}$S (volts)
Signal $^{32}$S (volts)
Axial detector mass scan (m/z)
0.0
0.5
1.0
1.5
2.0
2.5
3.0
0
5
10
15
20
25
30
32.87
32.88
32.89
32.90
32.91
32.92
32.93
32.94
32.95

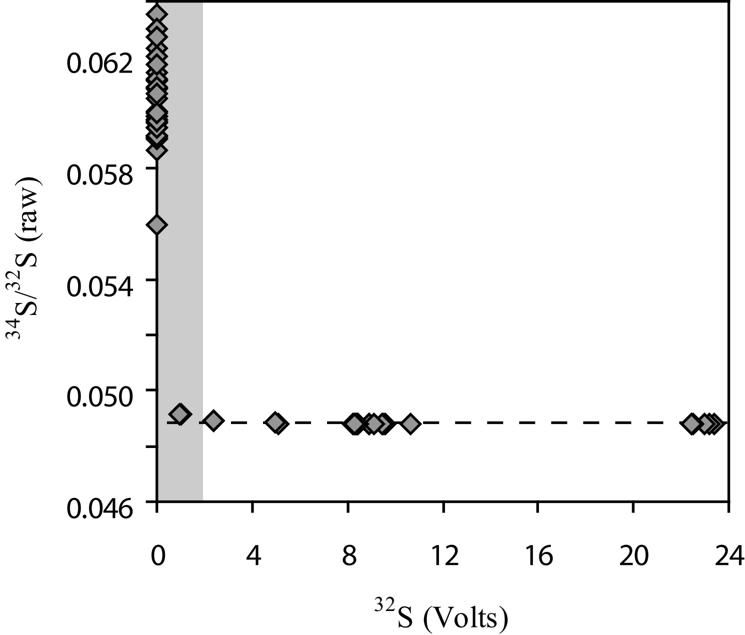
0.062
0.058
0.054
0.050
0.046
$^{34}S/^{32}S$ (raw)
0
4
8
12
16
20
24
$^{32}S$ (Volts)

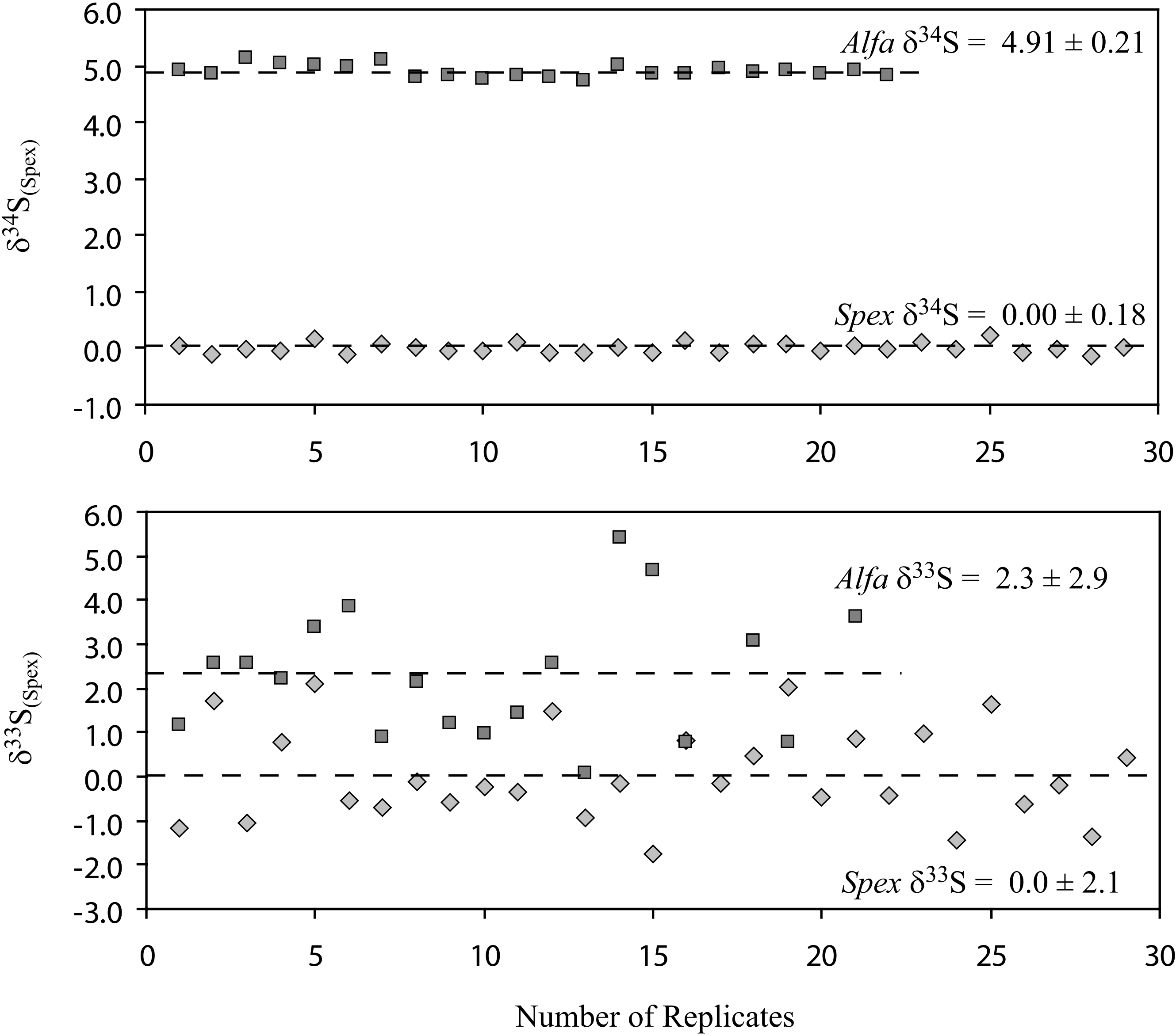
6.0
5.0
4.0
3.0
2.0
1.0
0.0
-1.0
δ34S(Spex)
*Alfa* δ34S = 4.91 ± 0.21
*Spex* δ34S = 0.00 ± 0.18
0
5
10
15
20
25
30
6.0
5.0
4.0
3.0
2.0
1.0
0.0
-1.0
-2.0
-3.0
δ33S(Spex)
*Alfa* δ33S = 2.3 ± 2.9
*Spex* δ33S = 0.0 ± 2.1
0
5
10
15
20
25
30
Number of Replicates

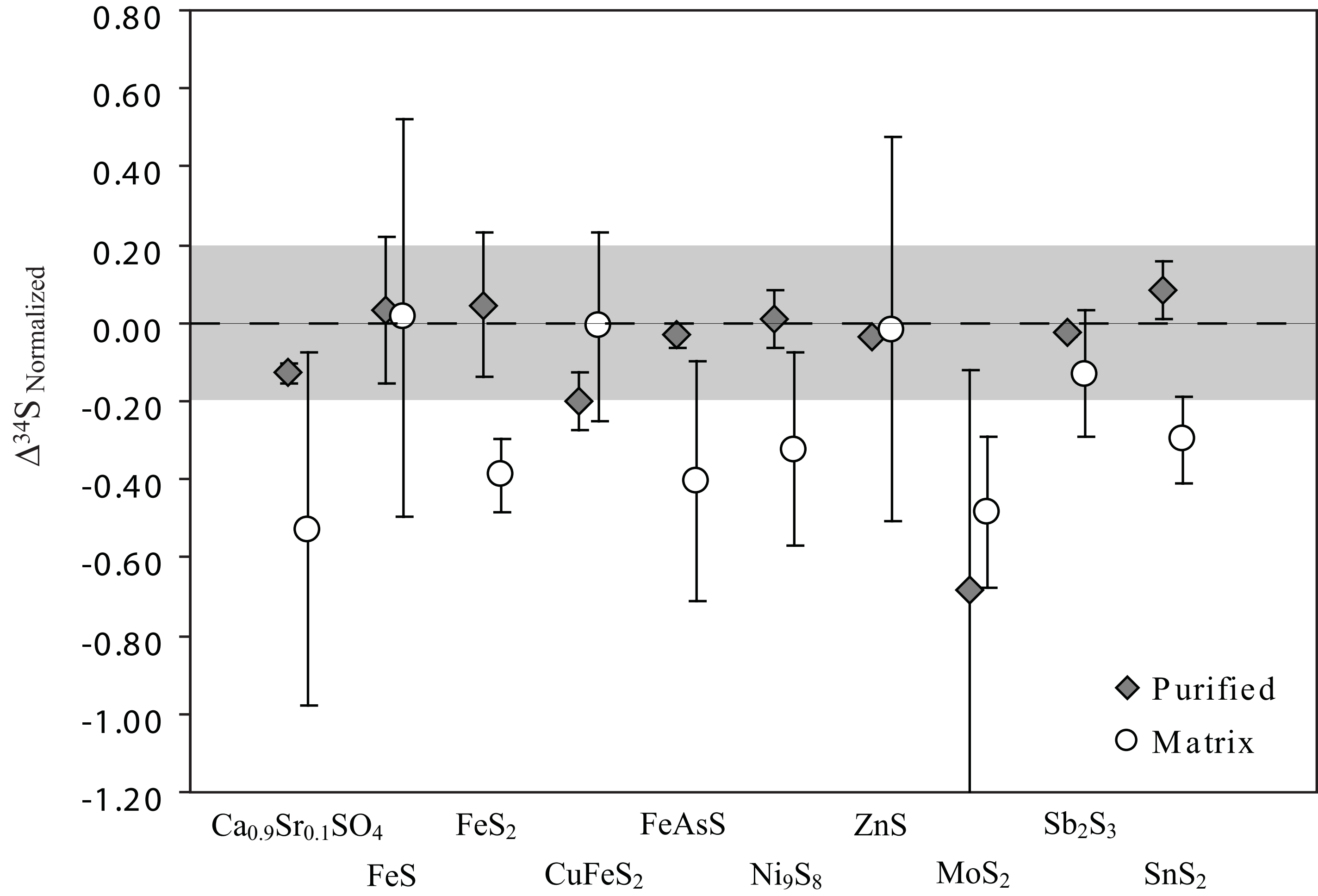
$\Delta^{34}S_{Normalized}$
0.80
0.60
0.40
0.20
0.00
-0.20
-0.40
-0.60
-0.80
-1.00
-1.20
$Ca_{0.9}Sr_{0.1}SO_4$
FeS
$FeS_2$
$CuFeS_2$
FeAsS
$Ni_9S_8$
ZnS
$MoS_2$
$Sb_2S_3$
$SnS_2$
Purified
Matrix

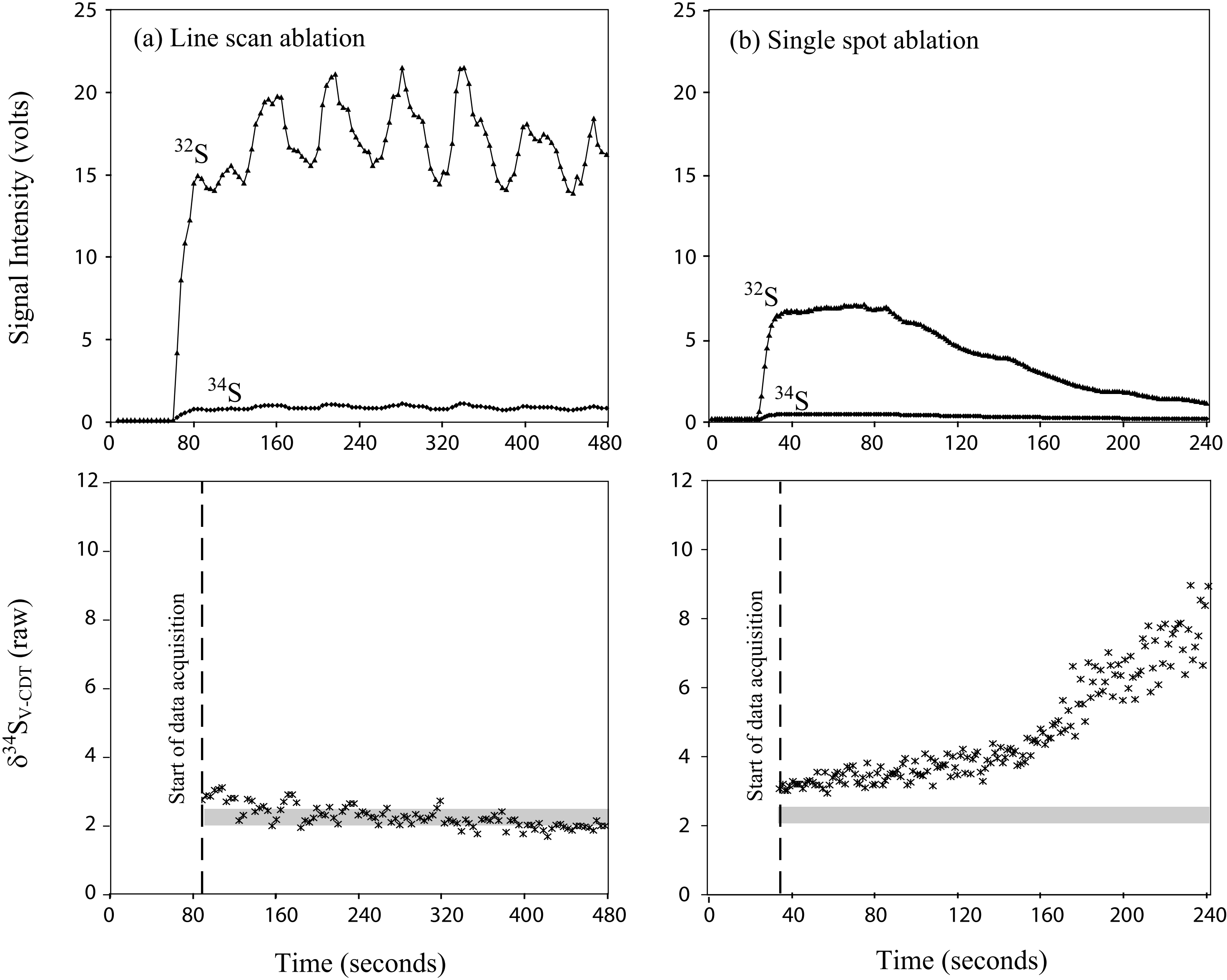
(a) Line scan ablation
(b) Single spot ablation
Signal Intensity (volts)
$^{32}$S
$^{34}$S
0
5
10
15
20
25
0
80
160
240
320
400
480
0
40
80
120
160
200
240
$\delta^{34}S_{V-CDT}$ (raw)
Start of data acquisition
0
2
4
6
8
10
12
Time (seconds)

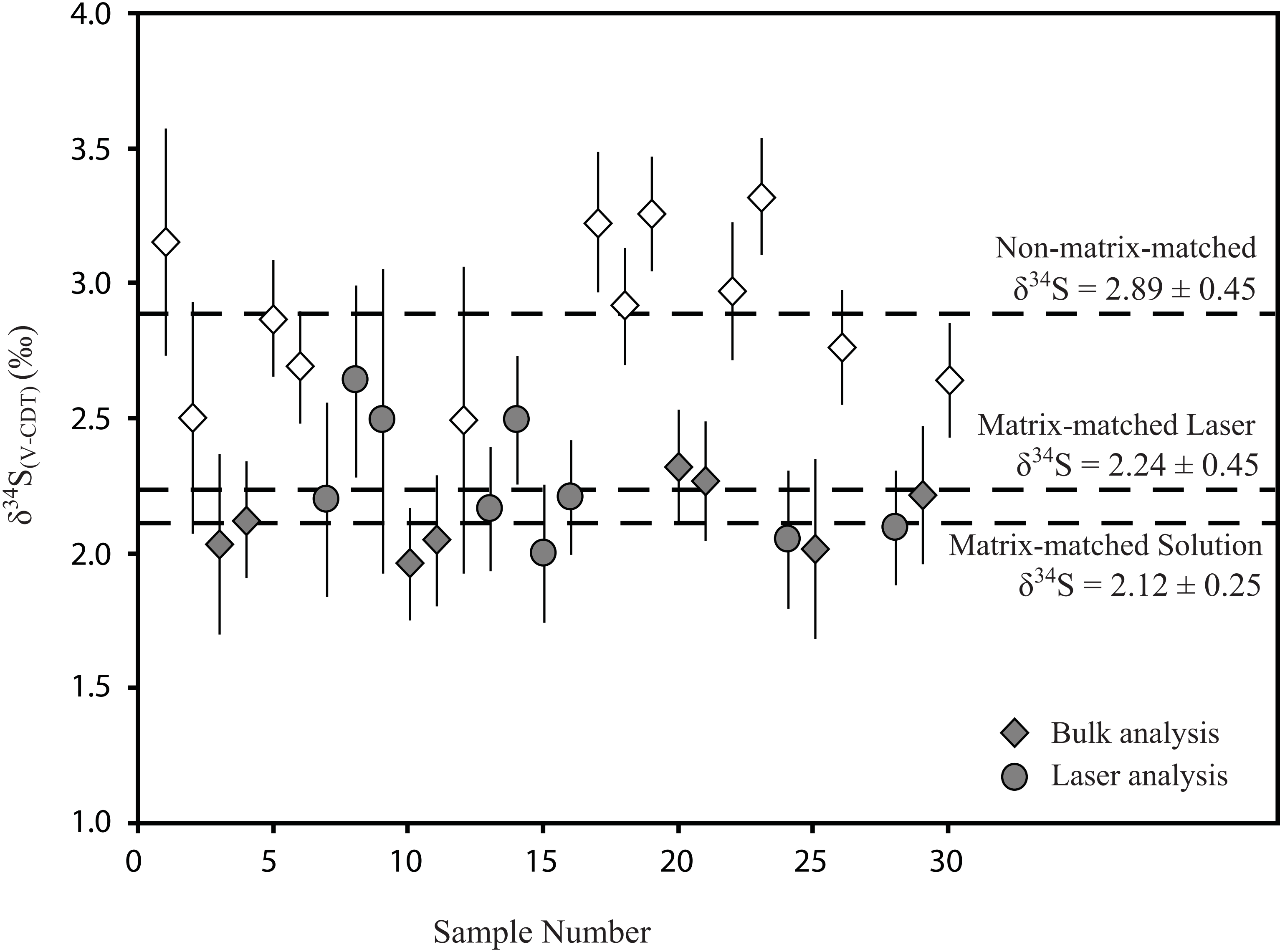
4.0
3.5
3.0
2.5
2.0
1.5
1.0
0
5
10
15
20
25
30
$\delta^{34}S_{(V\text{-}CDT)}$ (‰)
Sample Number
Non-matrix-matched
$\delta^{34}S = 2.89 \pm 0.45$
Matrix-matched Laser
$\delta^{34}S = 2.24 \pm 0.45$
Matrix-matched Solution
$\delta^{34}S = 2.12 \pm 0.25$
Bulk analysis
Laser analysis